

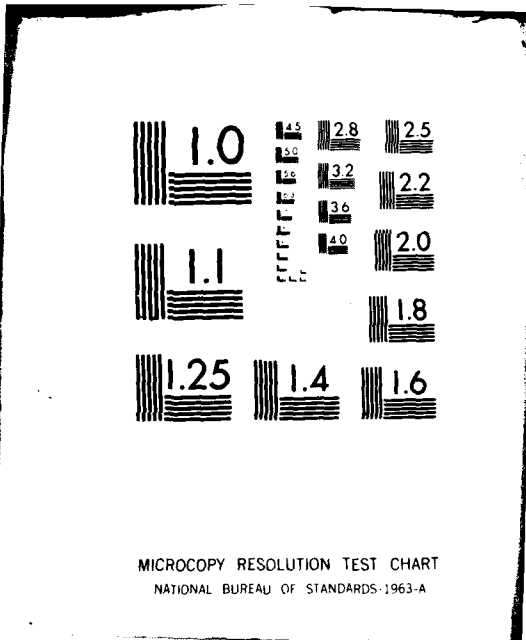
AD-A086 001

SCIENCE APPLICATIONS INC LA JOLLA CA F/0 80/6
REAL-TIME APPLICATIONS OF OPTICAL SIGNAL PROCESSING TO COMMAND --ETC (U)
APR 80 W STONER, E BARBER, F HERRIGAN F19628-78-C-0117
RADC-TR-80-86 NL

UNCLASSIFIED

Fig 1
Microfilm

END
DATE
FILED
8-80
DTIC



LEVEL

12

RADC-TR-80-86
Final Technical Report
April 1980



REAL-TIME APPLICATIONS OF OPTICAL SIGNAL PROCESSING TO COMMAND AND CONTROL COMMUNICATIONS

Science Applications, Incorporated

W. Stoner
E. Garber
F. Horrigan

G. Collins
J. Phelps

DTIC
ELECTE
S JUL 1 1980
C

ADA 086081

APPROVED FOR PUBLIC RELEASE; DISTRIBUTION UNLIMITED

AIR DEVELOPMENT CENTER
3353 BALDWIN ROAD
WRIGHT-PATTERSON AIR FORCE BASE, OHIO 45433

025

This report has been reviewed by the RADC Public Affairs Office (PA) and is releasable to the National Technical Information Service (NTIS). At NTIS it will be releasable to the general public, including foreign nations.

RADC-TR-80-86 has been reviewed and is approved for publication.

APPROVED:

W. J. Micelli

WILLIAM J. MICELLI
Project Engineer

APPROVED:

Clarence D. Turner

CLARENCE D. TURNER
Acting Director
Solid State Sciences Division

FOR THE COMMANDER:

John P. Huss

JOHN P. HUSS
Acting Chief, Plans Office

If your address has changed or if you wish to be removed from the RADC mailing list, or if the addressee is no longer employed by your organization, please notify RADC (RPO) Building 600, 21731, 11111. This will assist us in maintaining a current mailing list.

Do not return this copy.

UNCLASSIFIED

SECURITY CLASSIFICATION OF THIS PAGE (When Data Entered)

19 REPORT DOCUMENTATION PAGE		READ INSTRUCTIONS BEFORE COMPLETING FORM	
1. REPORT NUMBER RADC-TR-8D-86	2. GOVT ACCESSION NO. AD-A086 081	3. RECIPIENT'S CATALOG NUMBER	
6. TITLE (and Subtitle) REAL-TIME APPLICATIONS OF OPTICAL SIGNAL PROCESSING TO COMMAND AND CONTROL COMMUNICATIONS.		7. TYPE OF REPORT & PERIOD COVERED Final Technical Report, Apr 78 - Sep 79.	
7. AUTHOR(s) W./Stoner G./Collins E./Garber J./Phelps F./Horrigan		8. CONTRACT OR GRANT NUMBER(s) F19628-78-C-0117	
9. PERFORMING ORGANIZATION NAME AND ADDRESS Science Applications Incorporated/ 1200 Prospect St P O Box 2351 La Jolla CA 90238		10. PROGRAM ELEMENT, PROJECT, TASK AREA & WORK UNIT NUMBERS 62702F 46001924	
11. CONTROLLING OFFICE NAME AND ADDRESS Deputy for Electronic Technology (RADC/ESO) Hanscom AFB MA 01731		12. REPORT DATE Apr 80	
14. MONITORING AGENCY NAME & ADDRESS (if different from Controlling Office) Same		13. NUMBER OF PAGES 46	
		15. SECURITY CLASS. (of this report) UNCLASSIFIED	
		15a. DECLASSIFICATION DOWNGRADING SCHEDULE N/A	
16. DISTRIBUTION STATEMENT (of this Report) Approved for public release; distribution unlimited.			
17. DISTRIBUTION STATEMENT (of the abstract entered in Block 20, if different from Report) Same			
18. SUPPLEMENTARY NOTES RADC Project Engineer: William J. Micelli (ESO)			
19. KEY WORDS (Continue on reverse side if necessary and identify by block number) optical signal processing spread spectrum code acquisition incoherent optical processing optical A/D conversion			
20. ABSTRACT (Continue on reverse side if necessary and identify by block number) The program reported on in this final report was directed towards development of real-time optical signal processing for C ³ and radar applications. Specifically, these applications were A/D conversion, spread spectrum code acquisition and decoding, and clutter rejection in look-down radar. In the context of these applications and through discussions with RADC/ET, technical goals were framed, such as a goal of A/D conversion at 1 Ghz. New optical signal processing techniques			

DD FORM 1 JAN 73 1473 EDITION OF 1 NOV 65 IS OBSOLETE

UNCLASSIFIED

SECURITY CLASSIFICATION OF THIS PAGE (When Data Entered)

388862

UNCLASSIFIED

SECURITY CLASSIFICATION OF THIS PAGE(When Data Entered)

were conceived to meet the technical goals. These new approaches include a noncoherent kaleidoscope system for A/D conversion, and a noncoherent optical correlation technique which accommodates the bipolar and complex-valued signals encountered in spread spectrum communications and in radar. During the course of our program, determinations were made of the specific hardware best suited for the testing and demonstration of these novel approaches. These determinations were made by theoretical calculations and by consulting with the literature. Experimental tests of many subsystems, such as the noncoherent correlator optics and acousto-optic Bragg cells for introducing signals into the correlator in real-time, were tested at RADC/ET. Investigations were also made of computer generated holograms for use as pupil masks in the noncoherent correlator. The extensive literature on computer generated holograms was consulted, as well as the extensive literature on the phase retrieval problem, which is encountered during optimization of the pupil mask. New approaches to the problem of phase retrieval are proposed. The AFGL computer facility was investigated in terms of its usefulness in making computer generated holograms. Measurements were made and are reported here on the spatial resolution and distortion of the CRT plotter.

UNCLASSIFIED

SECURITY CLASSIFICATION OF THIS PAGE(When Data Entered)

E V A L U A T I O N

1. This is the final report of the contract. It considers real time application of optical signal processing for C³I from April 1978 to September 1979. The objectives were to investigate the implementation of optical processing techniques to various applications such as A/D conversion, and spread spectrum code acquisition and decoding. Various approaches, each employing optical techniques, were conceived for these applications. The significance of these new approaches is that they suggest ways of attaining previously unattainable goals.

2. This work relates to TPO R5D and is also applicable to TPOs 3 and 4. The value of the work is that it extends the versatility of optical processing techniques to potentially accommodate future C³I system requirements.

W. J. Micelli
WILLIAM J. MICELLI
Contract Monitor

Accession For	
W. J. MICELLI	<input checked="" type="checkbox"/>
DTIC TAB	<input type="checkbox"/>
Unannounced	<input type="checkbox"/>
Justification	
By	
Distribution/	
Availability Codes	
Avail and/or special	
A	

Table of Contents

1. Summary
2. Real-Time Applications of Optical Signal Processing to Command and Control Communications
3. Input Devices
4. Design of Pupil Masks
5. Image Pickup Devices
6. System Integration
7. List of Contributors
8. List of Publications
9. References

PRECEDING PAGE BLANK - NOT FILMED

1. Summary

The program reported on in this final report was directed towards the development of real-time optical signal processing for C³ and radar applications. Specifically, these applications were A/D conversion, spread spectrum code acquisition and decoding, and clutter rejection in look-down radar. In the context of these applications and through discussions with RADC/ET, technical goals were framed, such as a goal of A/D conversion at 1 Ghz. New optical signal processing techniques were conceived to meet the technical goals. These new approaches include a noncoherent kaleidoscope system for A/D conversion, and a noncoherent optical correlation technique which accomodates the bipolar and complex-valued signals encountered in spread spectrum communications and in radar. During the course of our program, determinations were made of the specific hardware best suited for the testing and demonstration of these novel approaches. These determinations were made by theoretical calculations and by consulting with the literature. Experimental tests of many subsystems, such as the noncoherent correlator optics and acousto-optic Bragg cells for introducing signals into the correlator in real-time, were tested at RADC/ET. Investigations were also made of computer generated holograms for use as pupil masks in the noncoherent correlator. The extensive literature on computer generated holograms was consulted, as well as the extensive literature on the phase retrieval problem, which is encountered during optimization of the pupil mask. New approaches to the problem of phase retrieval are proposed. The AFGL computer facility was investigated in terms of its usefulness in making computer generated holograms. Measurements were made and are reported here on the spatial resolution and distortion of the CRT plotter.

2. Real-Time Applications of Optical Signal Processing to Command and Control Communications

Our program of real-time optical signal processing was motivated equally by the drawbacks of conventional optical signal processing relative to competing technologies (digital, CCD, SAW) as by the well-known potential of optics for speed-of-light parallel processing of large blocks of data. In order to channel our efforts, two specific application areas were selected: (1) spread spectrum code acquisition and (2), clutter rejection in look-down radar. These specific applications provide a basis for setting realistic technical goals, and for assessing the success of our program.

The motivation to investigate optical A/D conversion was provided by the advances in digital processing over the last two decades, which suggest that digital techniques may eventually surpass the potential of optics. At present, the poor accuracy and low speed of A/D convertors is often the limiting factor in the real-time digital processing of communication and radar signals. Since A/D conversion is basically an analog process, and since the basic laws governing the acousto-optic and electro-optic interactions permit Gigahertz bandwidths and beyond, both the need for and the theoretical possibility of optical A/D conversion is uncontestable.

A large number of reasons motivated our emphasis of *noncoherent* rather than coherent optical processing. Foremost of these reasons is that the time is ripe for exploiting noncoherent optics: after a long period of unjustified neglect, new noncoherent processing concepts have been contributed by Lohmann,¹ Rhodes², and Stoner³, and compact, hybrid CCD-LED optical signal processing devices have been developed by Bromley and co-workers at NOSC⁴. In three specific areas, noncoherent optics surpasses coherent optics for signal processing:

- (1) noncoherent optics is inherently less prone to noise than coherent optics

- (2) noncoherent input devices (light modulators or displays) are generally simpler and more robust than coherent input devices
- (3) noncoherent optical systems tend to be less bulky and more robust than coherent optical systems.

It is obvious that these differences give noncoherent optics an advantage wherever weight, volume, ruggedness and reliability are factors... and they generally *are* factors in spread spectrum or radar applications.

Although we choose to pursue different noncoherent processing techniques than the NOSC group, their success with CCD-LED hybrids did influence us to investigate signal processing architectures which combine the strengths of acousto-optics Bragg cells, SAW filters and charge-coupled devices with optics. All three of these technologies assume important roles in conjunction with the noncoherent processor we studied under the contract. Acousto-optic Bragg cells provide real-time electronic-to-optical conversion. SAW bandpass filters are used to electronically post-process the output of the processor. In the future, CCDs will provide the basis for distortion free, high resolution 2-D input and output devices. Corner-turning CCDs will also be useful in applications such as noncoherent optical signal processing which require the re-formatting of data from 1-D to 2-D and vice-versa. In conjunction with all-electronic chirp z-transform devices, such corner-turning CCDs will soon provide a way of performing 2-D Fourier transforms without the bulk of coherent optics.⁵

2.1 Optical Analog to Digital Conversion

All electronic A/D convertors with sampling rates of 50 MHz are operational today. Sampling rates of 100 MHz at 4 to 6 bits represents the state of the art, and A/D convertors with 4 bits of precision at a 250 MHz sampling rate represents the most ambitious design goals presently on the drawing boards. Contrasting with these present and anticipated capabilities of electronics is the potential of optics for A/D conversion with precisions of something less than 10 bits and sampling rates of something less than 10 GHz. The goals chosen for our own program of optical A/D conversion are much more modest. Most C³ and radar applications operate with bandwidths of 500 MHz or less. By the Nyquist criterion, a

sampling rate of 1 Ghz is therefore sufficient to capture the signals. This led us to set a goal of 8 bits at 1 Ghz for our work.

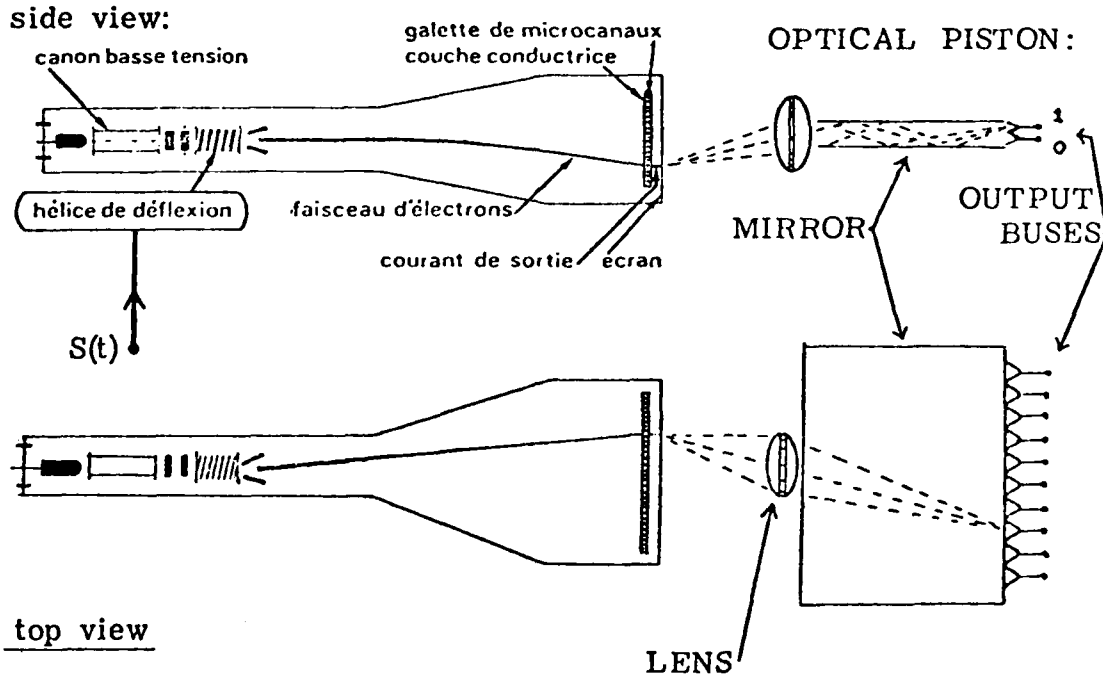
SAI proposes as a solution a hybrid system consisting of a traveling wave oscilloscope, and a kaleidoscope imaging system we have named the optical piston (Fig. 1). The function of the CRT is to display the waveform; the function of the optical piston is to map this display onto a pair of level sensing detectors. One optical piston provides only one bit of precision, but additional pistons may be added to obtain as many bits of precision as the resolution of the CRT display permits. Traveling wave deflection techniques are well developed, and permit fraction of a volt sensitivity at sweep rates fast enough to resolve a sine wave with a frequency of 6 Ghz.⁶ Despite the rapid sweep rate this requires, a bright display is achieved, because the electron beam is boosted in intensity with a microchannel plate just before it hits the CRT output phosphor. The optical piston sensitivity depends upon the distance separating its parallel mirrors; to obtain a binary code output of the CRT trace, a set of pistons varying in sensitivity by factors of 2 are required (Fig. 2).

Potential limitations of this approach are, (1) the bandwidth of detectors, (2) time-of-flight differences between the central and extreme portions of the CRT, (3) the risetime of the CRT output phosphor, and (4) the sweep rate of the CRT. These difficulties all point to the same ultimate limitation: a sample rate of ~ 10 Ghz. This is much faster than the 250 MHz rate presently envisioned for all electronic A/D convertors. The obvious drawback of our proposed A/D convertor is that it uses a bulky CRT. In principle electro-optic effects may be used to replace the CRT, but unless something is done to enhance the electro-optic effect, the resulting A/D convertor would have a sensitivity measured in tens of volts, rather than in millivolts.

2.2 Noncoherent Correlation

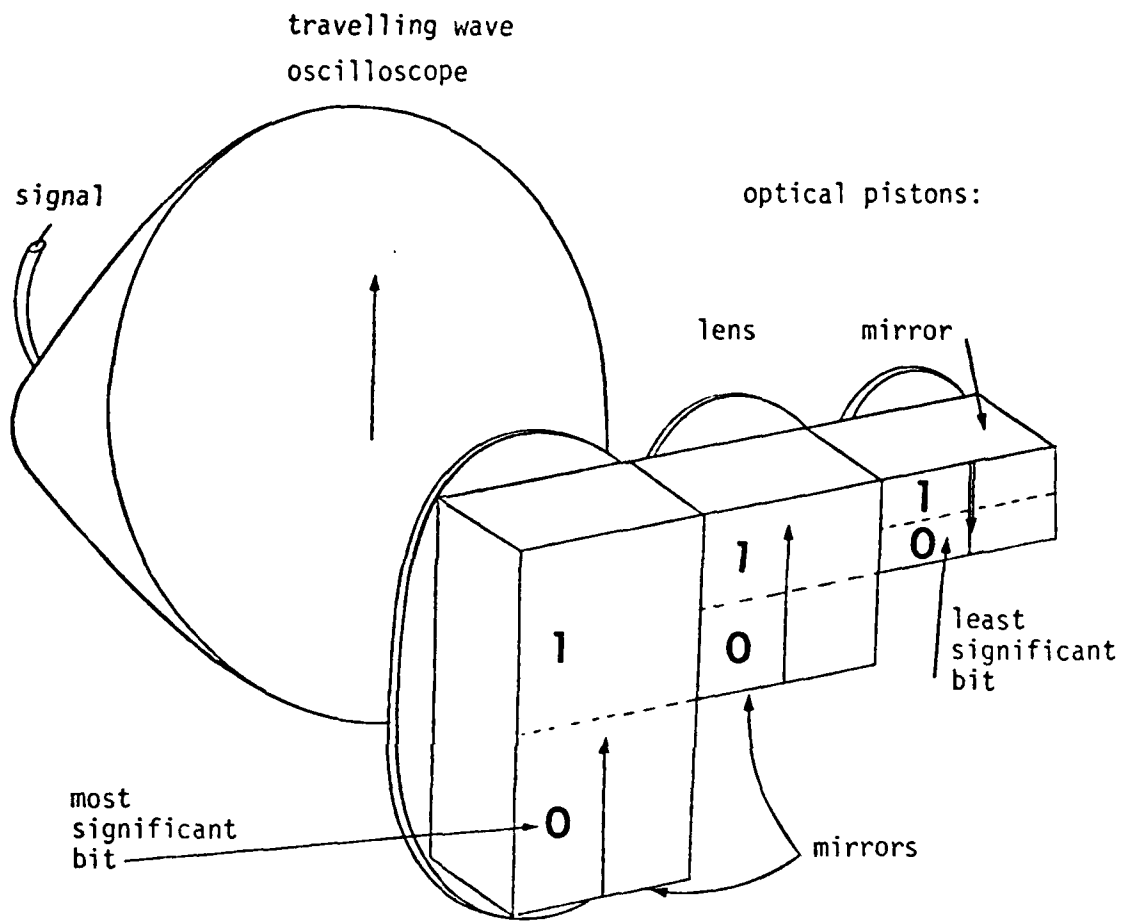
The basic operation achievable with noncoherent optics is *convolution*. Consider a system (Fig. 3) imaging in spatially noncoherent light: each bright point in the input plane is transferred into a blurred patch of light in the output plane (the system impulse response). By superposition, the

OPTICAL PISTON CONCEPT



(Source for wideband CRT: G. Pietri, "Contribution of the Channel Electron Multiplier to the Race of Vacuum Tubes Towards Picosecond Resolution Time", IEEE Tran. NS-24, p. 228, (Feb. 1977)).

Fig. 1



decimal value	Gray code representation
0	000
1	001
2	011
3	010
⋮	⋮

Fig. 2. Analog to Gray Code Conversion with Optical Pistons

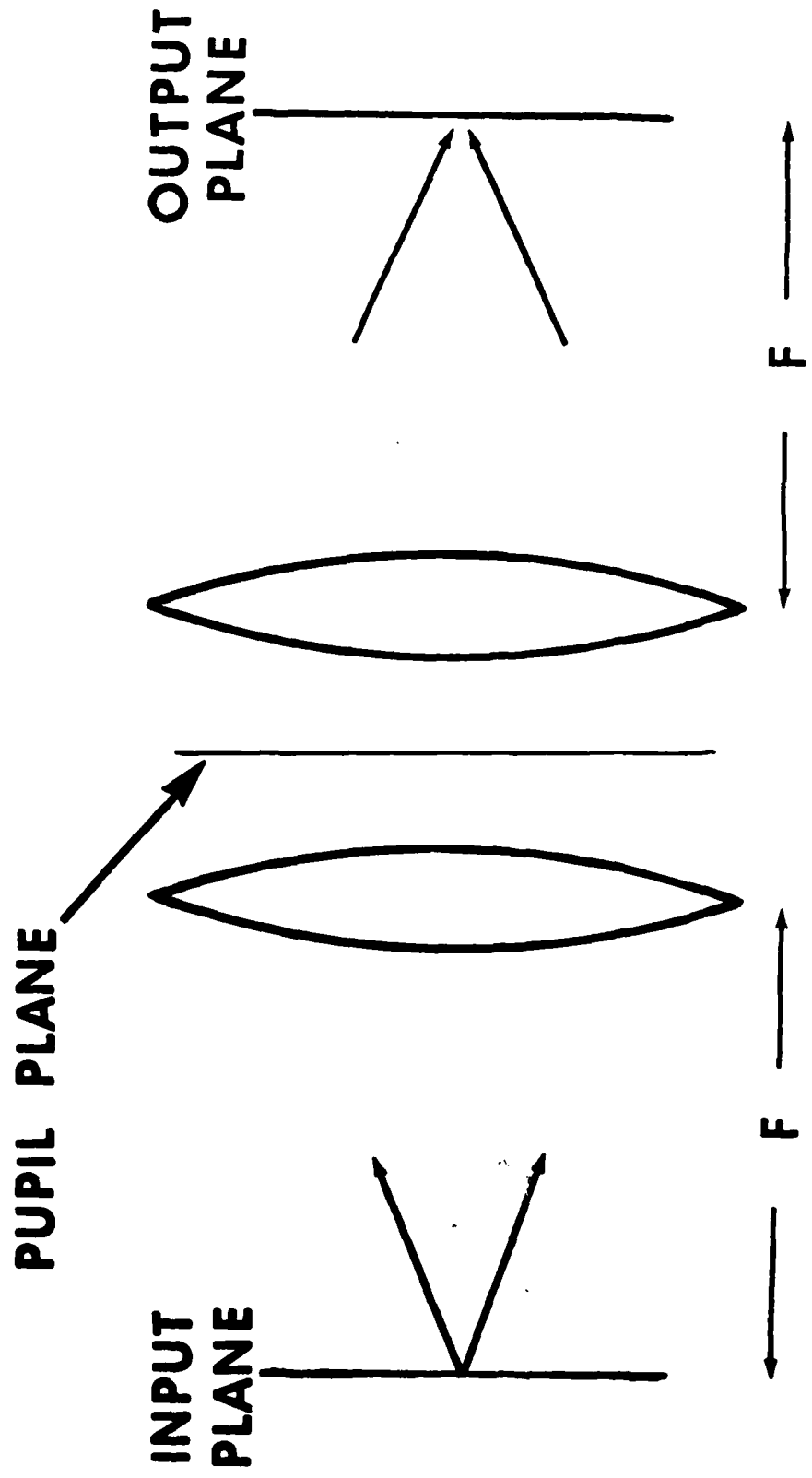


Fig. 3. Noncoherent Processor Optics

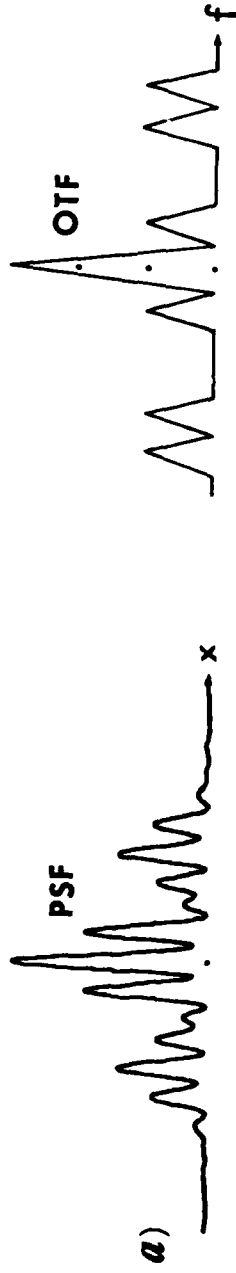
output image is therefore the convolution of the input intensity distribution with the impulse response. If a diffracting mask, $T(x)$, is inserted into the pupil plane of the imaging system, the impulse response may be shaped into a useful convolution function. We are mostly interested in shaping the impulse response by diffraction, but others have studied the use of coarse masks which shape the out-of-focus impulse response by simple shadowcasting.⁷ The disadvantage of shadowcasting is that it is limited to rather simple impulse responses; as the detail in $T(x)$ increases, diffraction effects cause the impulse response to deviate from that expected on the basis of geometric optics. So rather than fighting the effects of diffraction, we choose to use diffraction to shape the impulse response into a desired convolving function. This subject is discussed in depth in Section 4. We are interested here in another matter--the fact that intensity impulse responses are inherently non-negative. This was long assumed to prevent noncoherent optics from performing convolutions with bipolar or complex-valued functions. However, Lohmann,¹ Rhodes² and Stoner³ found a technique which circumvents the non-negative constraint on the impulse response. This technique is to employ a carrier frequency to represent the phase of the convolving function. Although a temporal carrier may be used, we shall only discuss the use of a spatial carrier. The idea is most easily discussed through an example (Fig. 4). Consider the bipolar signal in Fig. 4c. If it is placed on a frequency offset (heterodyned) it may assume the disguised form in Fig 4b. Since the heterodyned signal now consists solely of higher frequency components, it may be reversibly combined with low frequency components as in Fig 4a; by simple high-pass filtering it is possible to recover the signal in Fig 4b. Notice, however, that the signal in Fig 4a is *non-negative*. By this series of simple steps (1) heterodyning and (2) addition of a low frequency positive bias term it is possible to represent any bandlimited bipolar or complex-valued signal as a non-negative signal.

Although we have singled out the impulse response for our discussion of non-negativity, the input as well as the output of a non coherent imaging system are also non-negative. We have just seen that this is really no limitation: a bipolar or complex valued signal may be represented at the input by means of a frequency offset and a positive bias term. The really

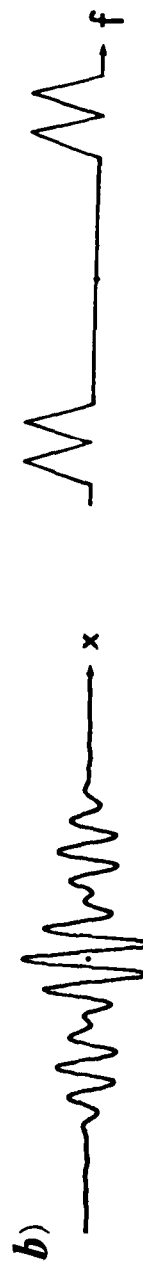
AN EXAMPLE OF ELECTRONIC POSTPROCESSING

SPATIAL DOMAIN

FREQUENCY DOMAIN



AFTER BANDPASS FILTERING:



AFTER DEMODULATION:

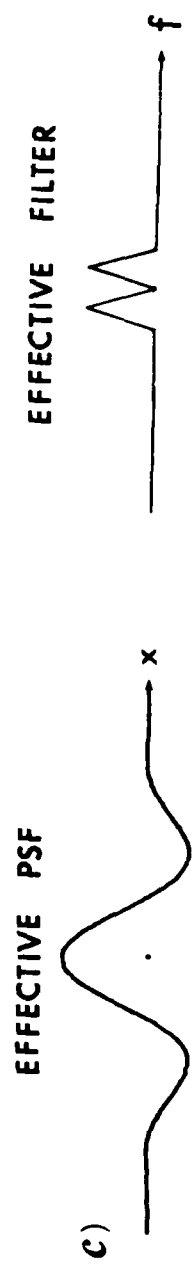


Fig. 4

useful fact, however, is that the convolution property of noncoherent optics extends to the convolution of bipolar or complex-valued signals which are represented by the frequency offset trick as non-negative functions. This is best seen with reference to Fig 5. Suppose we have an intensity image with a low frequency spectrum as in part (a). A frequency offset may be applied to this image by masking it with a Ronchi grating as shown in part (b). A imaging system with a spatial frequency offset impulse response will pass spatial frequencies around "dc" and also around the spatial frequency offset. The resulting output image consists of a conventional image composed of the spatial frequencies about "dc" and also a frequency offset image which corresponds to the convolution of the frequency offset components of the input image and the impulse response. This desired convolution may be recovered by detecting the output image with a raster scanning device, passing this raster signal through a bandpass SAW filter, and then heterodyning the output of the SAW filter back to baseband. Fig. 6 shows a block diagram of such a hybrid processor. Since correlations are basically the same as convolutions (only a simple change of coordinates is involved) it is possible to perform the correlation of a known signal (as in code correlation or in clutter rejection) with an input signal using this hybrid processing approach. The known signal must first be represented as the impulse response of the imaging system by means of an appropriate mask, $T(x)$, placed in the pupil. This question is studied in Section 4. Section 3 takes up the choice of input device, and Section 5 the choice of image pickup device. The overall system is discussed in Section 6.

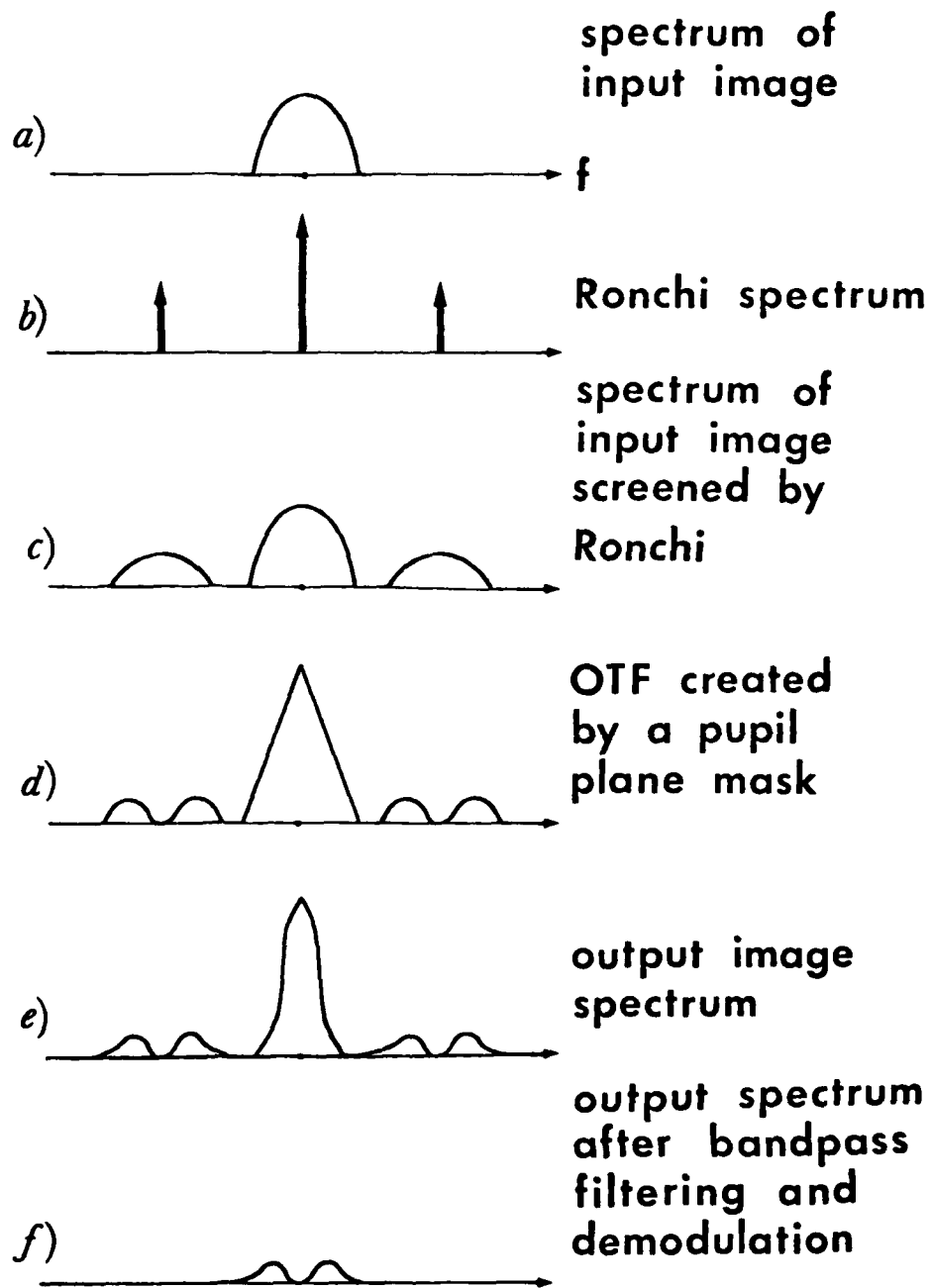


Fig. 5. Frequency Domain Viewpoint

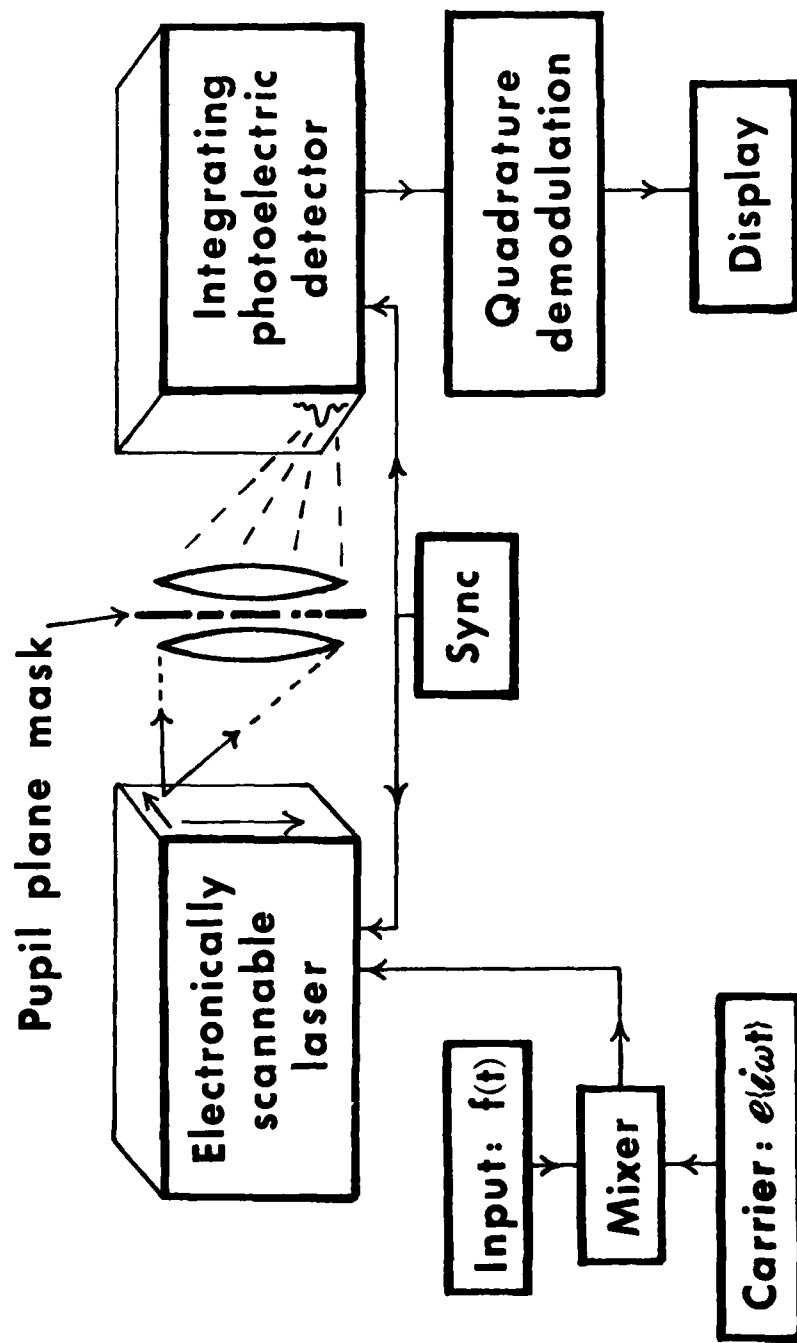


Fig. 6. Block Diagram of Noncoherent Processing System

3. Input Devices

One of the most persistent barriers to the widespread use of coherent optical processing has been the lack of high quality, real-time replacements for photographic film as an input medium. Our program of noncoherent optical processing is motivated in part by the fact that noncoherent processing relaxes the requirements on input devices. Whereas optical phase noise or distortion has a disastrous effect on a coherent input image, it has no effect at all on intensity, and only the intensity distribution is relevant in noncoherent optics.

Despite this fundamental advantage, one does not find advertisements for "noncoherent light valves," and yet a number of coherent light valves *are* commercially available: General Electric light valve, Hughes liquid crystal light valve, Science Applications, Inc. thermoplastic modulator, the Itek PROM,... These input devices exist because coherent optical processing enjoys a lead time of thirty years, while noncoherent approaches for processing of bipolar or complex valued data are barely three years old.

The strongest candidate noncoherent input device is a laser scanner. Though ultimately derived from a laser, a scanned display is spatially incoherent, because only one element of the display is "on" at a time. Before treating laser scanners in detail, we briefly discuss the other possible noncoherent input devices we have identified during the contract (Table 1).

Rare earth phosphor cathode ray tube displays are capable of operating at video rates, and probably at much higher rates such as 100 MHz. This high bandwidth potential is suggested by the development of traveling wave oscilloscopes with 6 GHz of bandwidth. Microchannel plate electron multipliers have made it possible to greatly increase the sweep rate of cathode ray tubes because the electron beam may be greatly intensified with a microchannel plate just before it hits the output phosphor to

Table 1

Electronic Input Devices
For Noncoherent Processors

- CRT Based
 - Rare earth phosphors
 - Dark trace screen (KCl, sodalite)
 - Phase or birefringence modulating devices intended as inputs for coherent optical processors, using schlieren or crossed polarizers
 - Electron beam pumped scannable laser
- Laser Scanner
- CCD Addressed (future possibility)

compensate for the intensity loss that otherwise would go hand-in-hand with the increase in sweep rate.⁶ On the negative side, it must be pointed out that rare earth phosphors while relatively narrowband as phosphors go, still have linewidths of .002 to .005 micron (Fig. 7).⁸ This about ten times larger than is desired. If filtration is used to reduce the linewidth, an unacceptable loss of intensity may occur. A further drawback is that no ready market for single phosphor cathode ray tubes exists, and so a special order would have to be placed to have such a tube fabricated. The fabrication techniques in themselves, however, have been very well developed, since ordinary color television tubes are more sophisticated than the single phosphor device needed for noncoherent optical processing.

Many of these remarks also apply to dark trace cathode ray tubes. In this type of tube a cathodochromic material, such as KCL or sodalite is used instead of a phosphor.^{9,10} Under electron bombardment cathodochromic materials turn from a translucent state to an absorbing state, because F-centers are created.¹¹ It is possible to use this effect in either a reflection or transmission read-out mode, but transmission provides the highest contrast. In noncoherent optical processing applications the cathodochromic screen might be back-lit with a diffuse mercury arc lamp or with a tilting beam laser illuminator. Laser light is coherent, but effectively noncoherent illumination may be synthesized if the incidence angle rotates relative to both the x and y axes during the integration period of the output detector.¹²

The cathodochromic image is persistent, and before a new frame of data may be displayed it is necessary to erase the screen. Either optical or thermal erasure may be used. Optical erasure is nearly instantaneous, but it cannot be used to erase the type of F-centers which provides the highest contrast. Thermal erasure times of less than 2 seconds have been demonstrated at RCA in an experimental transmission-mode device.¹⁰ As is the case with rare earth phosphor displays, cathodochromic displays are not commercially available. However, they are reported to be inherently simple and are expected to be inexpensive to manufacture.

Under electron bombardment, direct bandgap semiconductors are capable of laser action. This effect has been used to create a scannable laser, by attaching a single crystal CdS wafer on the inside surface of a cathode

SPECTRAL-ENERGY DISTRIBUTION CHARACTERISTICS
OF PHOSPHOR TYPE P45

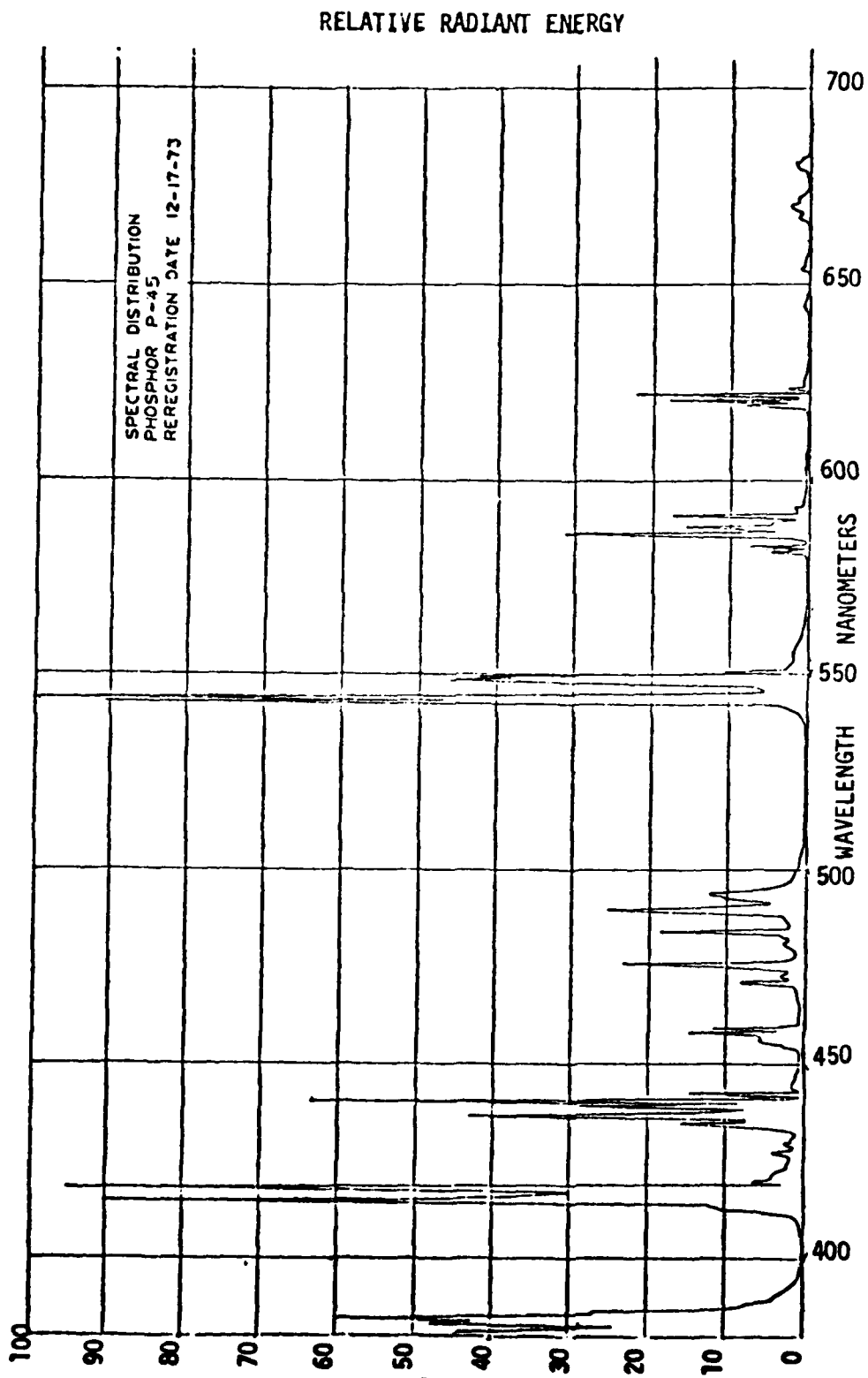


Fig. 7. Typical Rare-Earth Phosphor Spectrum (Taken from Ref. 8)

ray tube window. The lasing region may be made to scan across the face of the CdS wafer by sweeping the electron beam, because lasing occurs only where the electron beam is focused. The emitted radiation is narrow-band, and is typically spread (by diffraction) over an angle of .2 radians. A device constructed at 3M Company provided more than 1000x1000 addressable spots of high intensity.¹³ This type of input device appears to be an excellent candidate for noncoherent processing, but once again we find that nothing is available commercially.

Coherent light valves may also be used as noncoherent input devices. There are at least two ways of noncoherently reading out such displays: (1) schlierin projection may be performed with a small noncoherent source or (2) a tilting laser beam may be used to synthesize noncoherent illumination over the integration period of the output detector. Method (1) is the way the General Electric projection television system works. This method has the drawback that it is difficult to achieve complete incoherence over the display. The large area source needed to produce spatially incoherent illumination conflicts with the geometry of the schlierin projection system. Method (2) has been proposed by Chavel.¹² It is complicated by the fact that the laser beam must be independently tilted along two orthogonal axes. One way to achieve the necessary tilting is by imaging the coherent light valve onto a slowly twisting mirror, and re-imaging the reflected light onto a second mirror which rotates more rapidly along the orthogonal axis. The image reflected off this second mirror may be directed into the noncoherent processor because the tilting of the laser beam wipes out its spatial coherence. The drawback of this technique is that one of the mirrors is required to oscillate at a very high frequency in order to wipe out spatial coherence over the period of a single video frame. Although it is possible to replace one or both of the mirrors with acousto-optic Bragg cells, this approach does not use the coherent light valve to advantage; the acousto-optic Bragg cells may be used as a laser scanner all by themselves.

Laser scanners are the only candidate input devices which are commercially available and do not require auxiliary supporting systems such as schlieren optics or tilting laser beam illuminators. Two dimensional scanners may be constructed with moving mirrors, acousto-optical Bragg cells, rotating computer generated holograms or combinations of these components.

Since many of the components for an acousto-optic modulator-scanner were already available at RADC/ET, we looked into assembling these components into an input device for noncoherent optical processing. Three salvaged acousto-optical Bragg cells were investigated. Plausible values for the operating frequencies of these cells were determined by measuring their impedances on an AC bridge. The cells were then tested for diffraction efficiency by driving them with 1-2 watts of power at the frequencies where they were found to be resistive. An Isomet cell was found to operate best around 75 ± 2.5 MHz, a Datalight cell best around 70 ± 1.5 MHz and a Martin-Marietta cell best around 40 ± 5 MHz. At the 1-2 watt power level these cells achieved diffraction efficiencies of roughly 50%. If one cell operated as the modulator, and the other two as horizontal and vertical deflectors, the overall light efficiency would be roughly 10%. Galvanometer moving mirror scanners are relatively cheap and sufficiently fast to use for the vertical deflection.¹⁴ This is the approach we recommend, because it leads to a more acceptable overall light efficiency.

4. FILTER AND PUPIL MASK DESIGN

In every branch of signal processing, analog as well as digital, a considerable effort has been devoted to the design of filters for linear signal processing. In digital processing the effects of roundoff, sampling parameters, aliasing, interpolation (for conversion between polar and cartesian coordinates in sensor array processing, etc.), and the pros and cons of direct convolution versus frequency filtering using DFTs (discrete Fourier transforms) must all be carefully considered.¹⁵ Similar problems arise in analog signal processing, and in addition one must contend with device limitations such as charge transfer inefficiency in CCDs, sound wave attenuation, reflection and diffraction in SAWs, etc. Although work is still going on, progress in understanding the underlying physics of SAW devices has been sufficient to permit analytic design.¹⁶ Our objective here is to provide the foundation for such design techniques in noncoherent pupil mask processors.

Convolution is the signal processing operation most naturally performed by noncoherent optics. Indeed, the process of image formation is nothing more than the convolution of the input intensity $i(x,y)$ with the point spread function $h(x,y)$ of the imaging system (Fig. 3).

$$o(x',y') = \int \int i(x,y) \cdot h(x'-x,y'-y) dx dy, \quad (1)$$

where $o(x',y')$ denotes the output intensity image. Fourier transforming (1) provides a frequency domain representation of the imaging process:

$$O(f_x, f_y) = I(f_x, f_y) \cdot H(f_x, f_y), \quad (2)$$

where the frequency response $H(f_x, f_y)$ is the Fourier transform of $h(x,y)$. In the parlance of noncoherent optics, $H(f_x, f_y)$ is the OTF or optical transfer function.¹⁷ The next question is how to implement a given $H(f_x, f_y)$ and $h(x,y)$. This is done by inserting an appropriate phase and

amplitude modulating transparency, $T(x,y)$ into the pupil plane of the processor. Because the effect of a given transparency depends upon the focal length F of the processor optics and the wavelength λ of the illumination, it is useful to define new variables $\mu = x/F\lambda$ and $\nu = y/F\lambda$, and to represent the transparency by

$$p(\mu,\nu) = p\left(\frac{x}{F\lambda}, \frac{y}{F\lambda}\right) = T(x,y). \quad (3)$$

One calls $p(\mu,\nu)$ the pupil function. H and h are related to p by the following:¹⁷

$$h(x,y) = \left| \iint p(\mu,\nu) \exp(+2\pi i(\mu x + \nu y)) \, d\mu d\nu \right|^2 \quad (4)$$

$$H(f_x, f_y) = \iint p(f_x + \mu, f_y + \nu) p^*(\mu,\nu) \, d\mu d\nu \quad (5)$$

(Obviously, these relationships are connected with one another by the Fourier convolution theorem.) Given the Fourier transform pair H and h , either Eq. (4) or Eq. (5) must be inverted to find $p(\mu,\nu)$. As we shall show, there is some ambiguity introduced by the nonlinearity of these relationships which suggests that many different $p(\mu,\nu)$ correspond to a given H and h . If such freedom does exist it can be used to select a $p(\mu,\nu)$ which is all phase or all amplitude, or a $p(\mu,\nu)$ which is quantized to a few levels of phase and/or amplitude.

Since $h(x,y)$ represents an intensity it is derived from an amplitude:

$$h(x,y) = |A(x,y)|^2, \text{ where} \quad (6)$$

$$A(x,y) = |A(x,y)| \exp(i\phi(x,y)), \text{ and} \quad (7)$$

$$A(x,y) = \iint p(\mu,\nu) \exp(+2\pi i(\mu x + \nu y)) \, d\mu d\nu \quad (8)$$

It is easy to solve for $|A|$ by taking the square root of h . It may also

seem easy to multiply $|A|$ by an arbitrary phase factor, $\exp(i\phi(x,y))$, and to inverse transform to obtain $p(u,v)$. The catch is that $p(u,v)$ cannot go on forever, but must be zero for $u,v \gtrsim R/F\lambda$, where R is the radius of the processor lenses. Arbitrary choices of $\phi(x,y)$ lead to discontinuities in $A(x,y)$ which correspond to a $p(u,v)$ of infinite extent.¹⁸ If only the central region of this $p(u,v)$ is used, a smoothed approximation to $A(x,y)$ is obtained which will not exactly satisfy Eq. 6. It is clear that we need both a way of specifying good choices of $\phi(x,y)$ and a criterion for assessing the approximations we achieve to h and H .

The design techniques we require are quite closely related to the techniques developed to design computer generated holograms (CGH). The earliest CGHs were simply mimics of the holograms which can be obtained experimentally; in particular, they used a spatial carrier frequency to encode phase. An undesirable limitation of this early approach is that the spatial carrier uses up a large fraction of the plotting capacity of the plotter or scanner which is used to compose the hologram. Moreover, the diffraction efficiency of thin amplitude holograms is poor. Even earlier work of Tsujiuchi¹⁹ demonstrated that true complex wave modulation was achievable by forming a sandwich filter consisting of an amplitude modulating transparency and a phase modulating transparency. Registration of the transparencies is critical, however. Chu and Fienup²⁰ recently found a practical way to produce such phase and amplitude sandwiches. Multi-emulsion film, such as Kodak Kodachrome color reversal film, contains film layers which can be separately exposed, by using exposures with different colors. After development, the resulting blue and red dye images can be used to control the amplitude and phase of a transmitted HeNe (red light) beam, because the red dye predominantly influences the phase of the transmitted beam, while the blue dye predominantly influences its amplitude. Because no spatial carrier is needed to encode phase, the image is produced on-axis and so this type of CGH contains no trace or analog to the reference beam of conventional holography. Hence the name ROACH --- Referenceless On-Axis Complex Hologram. Fienup's work²¹ was directed towards using ROACHs in

computer memories. This application demands good image fidelity, in order to achieve low bit error rates. For this reason careful work was done to improve the process of making good holograms. The photographic process had to be well understood, and beyond this, techniques were studied which attempt to find good choices for the phase, $\phi(x,y)$, of the holographically constructed image wavefront $A(x,y)$. Fienup's work followed up on an iterative phase construction technique developed by Gerchberg and Saxon.²²

Many pupil functions for noncoherent optical processing have already been found without avail to an arsenal of phase construction techniques.²³ However, such an arsenal is extremely desirable, because noncoherent processing cannot be fully exploited without techniques for finding the optimal (in some sense to be determined) pupil function $p(u,v)$ for implementing a given $H(f_x, f_y)$ and $h(x,y)$. For this reason we took a broad look at the phase construction problem. It occurs in many disciplines, including electrical engineering, radioastronomy, speckle interferometry, x-ray crystallography, elementary particle physics, and optics. We sought both general solutions to the problem, and specialized techniques applicable to restrictive cases. A number of very promising phase construction techniques were conceived or identified from the literature during the contract. As yet, no application of these techniques to pupil function generation has been attempted, but the way is now clear to do so.

The outline below gives an overview of the discussions that follow.

General Techniques For Phase Construction

- Given only $h(x)$ or $h(x,y)$:
 - 1-D case: analyticity and Hilbert transforms
 - our heuristic extension into 2-D
 - the feasibility of large-scale optimization

- Given $h(x,y)$ and a guess for $|p(u,v)|$:

- Gerchberg-Saxon iteration
- Dallas' algebraic solution

Specific Techniques of Interest in Signal Processing

- techniques developed by x-ray crystallographers
- windowing in conjunction with small scale optimization

4.1 General Techniques for Phase Construction

4.1.1 The Use of Analyticity

This approach to the phase problem follows contributions made almost simultaneously by Walther and O'Neill,^{24,25} Hofstetter,²⁶ and Goldberger, Lewis and Watson.²⁷ It is interesting that these scientists are respectively from the disciplines of optics, electrical engineering, and physics. They followed a general approach first introduced by physicists studying scattering (Kramers and Kronig)²⁸ and by electrical engineers studying electrical filters (H.W. Bode).²⁹ A serious limitation of this approach is that it covers only the one-dimensional case, but we have developed a heuristic extension for the two-dimensional case. In order to present our extension, it is necessary to briefly explain the one-dimensional case. We strive here to convey the flavor. Our introduction should make the extensive literature on the subject more accessible.

Suppose we have an amplitude $A(x)$ with Fourier transform $p(\mu)$, $p(\mu) = 0$ for $|\mu| > c$. $A(x)$ may be analytically continued into the complex plane by replacing x in Eq. 8 by $z = x + iy$:

$$A(z) = \int_{-c}^c p(\mu) \exp(2\pi iz\mu) d\mu \quad (9)$$

It can be shown that $A(z)$ is analytic over any finite region of the complex plane, and that $A(z)$ may be expressed as a product over its

zeros, z_i , in the complex plane:

$$A(x) = \exp(\beta_0 + \beta_1 iz) \prod_i \left(1 - \frac{z}{z_i} \right) \exp\left(\frac{z}{z_i}\right) \quad (10)$$

Example: $A(x) = \frac{\sin(\pi x)}{\pi x}$; $\rho(\mu) = 1$, $|\mu| < \frac{1}{2}$, $\rho(\mu) = 0$, $|\mu| > \frac{1}{2}$:

$$A(z) = \int_{-\frac{1}{2}}^{+\frac{1}{2}} \exp(2\pi iz\mu) d\mu = \frac{\sin(\pi(x+iy))}{\pi(x+iy)} = \frac{\sin \pi x \cosh \pi y + i \cos \pi x \sinh \pi y}{\pi(x+iy)}$$

$$A(z) = \frac{\sin(\pi z)}{(\pi z)} = \prod_{n=-\infty}^{n=+\infty} \left(1 - \frac{z}{n} \right) \exp\left(\frac{z}{n}\right)$$

Notice that this case is exceptional in that all of the zeros of $A(z)$ fall on the real axis: $z = 0, \pm 1, \pm 2, \dots, \pm n, \dots$

Since $h(x) = A(x) A^*(x)$, we may also analytically extend h into the complex plane:

$$h(z) = A(z) A^*(z^*), \quad (11)$$

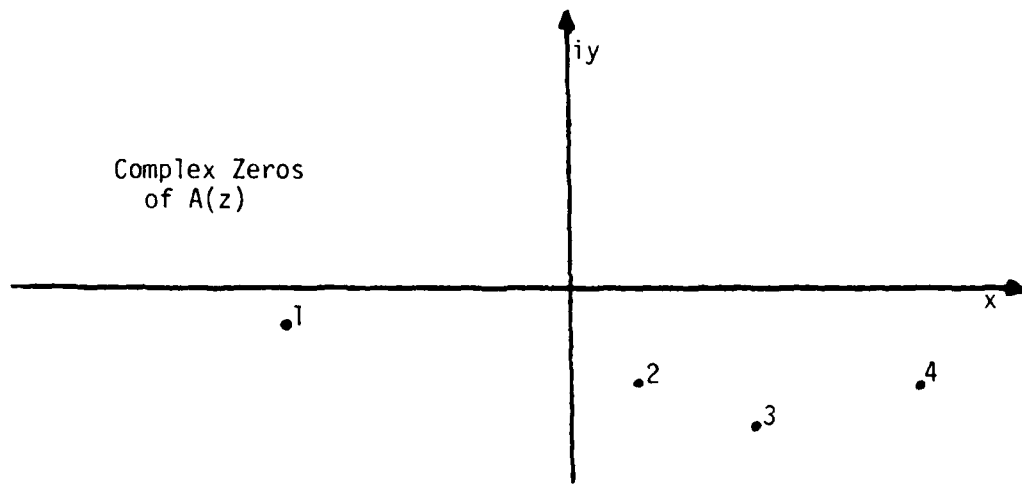
where z^* appears instead of z because this makes $A^*(z^*)$ a function of z . Clearly, $h(z)$ reduces to $|A(x)|^2$ as z approaches x . Plugging the expression for $A(z)$ in Eq. 10 into Eq. 11,

$$h(z) = \exp(2(\operatorname{Re} \beta_0) + 2(\operatorname{Re} \beta_1)z) \prod_i \left(\left(1 - \frac{z}{z_i} \right) \exp\left(\frac{z}{z_i}\right) \cdot \left(1 - \frac{z}{z_i^*} \right) \exp\left(\frac{z}{z_i^*}\right) \right), \quad (12)$$

one observes that wherever $h(z)$ has a zero at z_i , it also has a zero at z_i^* . If we were given Eq. 12 for $h(z)$, and asked to find $A(z)$, we would not know whether to choose the factor $\left(1 - \frac{z}{z_1} \right) \exp\left(\frac{z}{z_1}\right)$ or the

factor $(1 - \frac{z}{z_1^*})\exp(\frac{z}{z_1^*})$, or whether to choose $(1 - \frac{z}{z_2^*})\exp(\frac{z}{z_2^*})$ rather than $(1 - \frac{z}{z_2})\exp(\frac{z}{z_2})$, and so forth. For each i , an arbitrary choice may be made. No matter what choices are made, the resulting expression for $A(z)$ will still lead to the same expression for $h(z)$ as Eq. 12. Although the value of $h(x)$ remains the same, and the value of $|A(x)|$ remains invariant, the value of $A(x)$ generally changes, and therefore its Fourier transform $p(\mu)$ also generally changes. In exceptional cases, such as $A(x) = \sin(\pi x)/(\pi x)$, all of the zeros z_i turn out to be real, and in this case there is no difference between z_i and z_i^* .²⁵ then $A(x)$ and $p(\mu)$ are unique, except for trivial phase factors (since only the real part of β_0 and β , appear in Eq. 12, it is always possible to change the imaginary parts of β_0 and β , in the expression for $A(z)$). The process of changing from one choice of $A(z)$ to another by replacing $(1 - \frac{z}{z_i})\exp(\frac{z}{z_i})$ with $(1 - \frac{z}{z_i^*})\exp(\frac{z}{z_i^*})$ in Eq. 10 is called zero-flipping, because it exchanges a zero at z_i with its mirror image about the real axis, (Figure 8). Given $h(x)$, if we could only find one of the $A(z)$ we would have its zeros, z_i , and we could play the zero flipping trick to find any of the other $A(z)$ we wish. (Since the number of complex zeros may be zero, finite or infinite, there may be only one acceptable $A(x)$, a finite number, or an infinite number.)²⁵

An expression does exist for one of the $A(z)$. This special $A(z)$ has all of its zeros in the lower half plane. It is known as the minimum phase solution.³⁰ This term comes from electrical circuit theory. The time delay of an electrical impulse through a linear circuit is related to the phase of the filter frequency response. Of all the electrical circuits with the same frequency response magnitude, the one which introduces the least delay has the least phase variation. In our context, an analogous statement holds. The minimum phase $A(z)$ corresponds to the $p(\mu)$ which is maximally concentrated at $\mu=0$ in the following sense:



Complex zeros of:

$$A'(z) = A(z) \cdot \left[\frac{(1-z/z_3^*)}{(1-z/z_3)} \right]$$

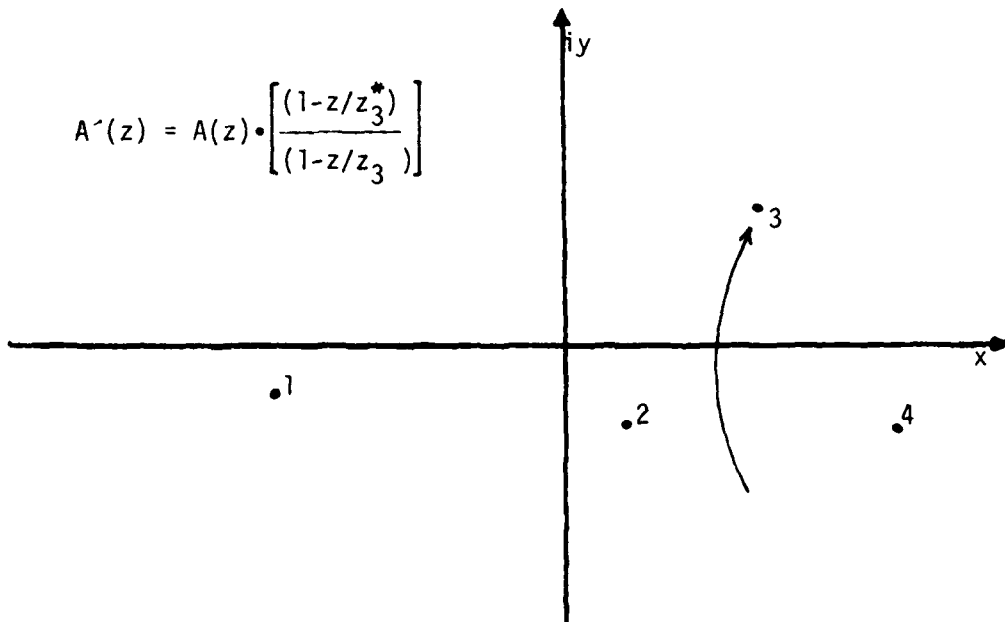


Fig. 8. An Example of Zero-Flipping

$$\int_0^a \min |p(\mu)|^2 d\mu > \int_0^a |p(\mu)|^2 d\mu \text{ for all } a. \quad (13)$$

The phase, $\phi(x)$, of the minimum phase amplitude, $A(x) = |A(x)| \exp(i\phi(x))$, is given by the Hilbert transform of $\log(|h(x)|^2)$:

$$\phi(x) = \frac{1}{\pi} \int_{-\infty}^{+\infty} \frac{\log(|h(y)|^2)}{(y-x)} dy \quad (14)$$

We now have a recipe for computing the set of $p(\mu)$ which correspond to a given $h(x)$: Use Eq. (14) to compute $A(x) = \sqrt{h(x)} \exp(i\phi(x))$. Fourier transform to obtain $p(\mu)$; then Laplace transform (Eq. 9) to obtain $A(z)$, the analytic continuation of $A(x)$. Compute the zeros of $A(z)$ out to a large value of $|z|$ (they all lie on the lower half plane). Obtain equally acceptable $A(z)$ by zero-flipping. Fourier transform the corresponding $A(x)$ to obtain new $p(\mu)$. Choose the $p(\mu)$ which is most easily fabricated.

4.1.2 Two Dimensional Extension

Given $h(x,y)$, fix y to obtain the one-dimensional function $h(x,y')$. Compute the zeros z_i of the corresponding analytically extended minimum phase amplitude, which we denote by $A(z,y')$. Consider $h(x,y'+\epsilon)$ for ϵ much less than the Nyquist sampling interval. By continuity, the zeros z_i of $A(z,y'+\epsilon)$ must approach the zeros of $A(z,y')$ as ϵ approaches zero. If one stacks up the complex planes for increments of y' , (Fig. 9), the locus of the z_i are continuous curved lines occupying the $\text{Imag}(z) < 0$ half of the three-dimensional space (z,y') . By continuity, these loci cannot end abruptly; however, they can move off towards infinite $|z|$. In this way it is possible for the character of the minimum phase $A(z,y')$ to vary with y' .

We have not carefully investigated the properties of the function $A(z,y')$. It is clearly a close cousin to the minimum phase amplitude in the one-dimensional case, and it limits to this amplitude if

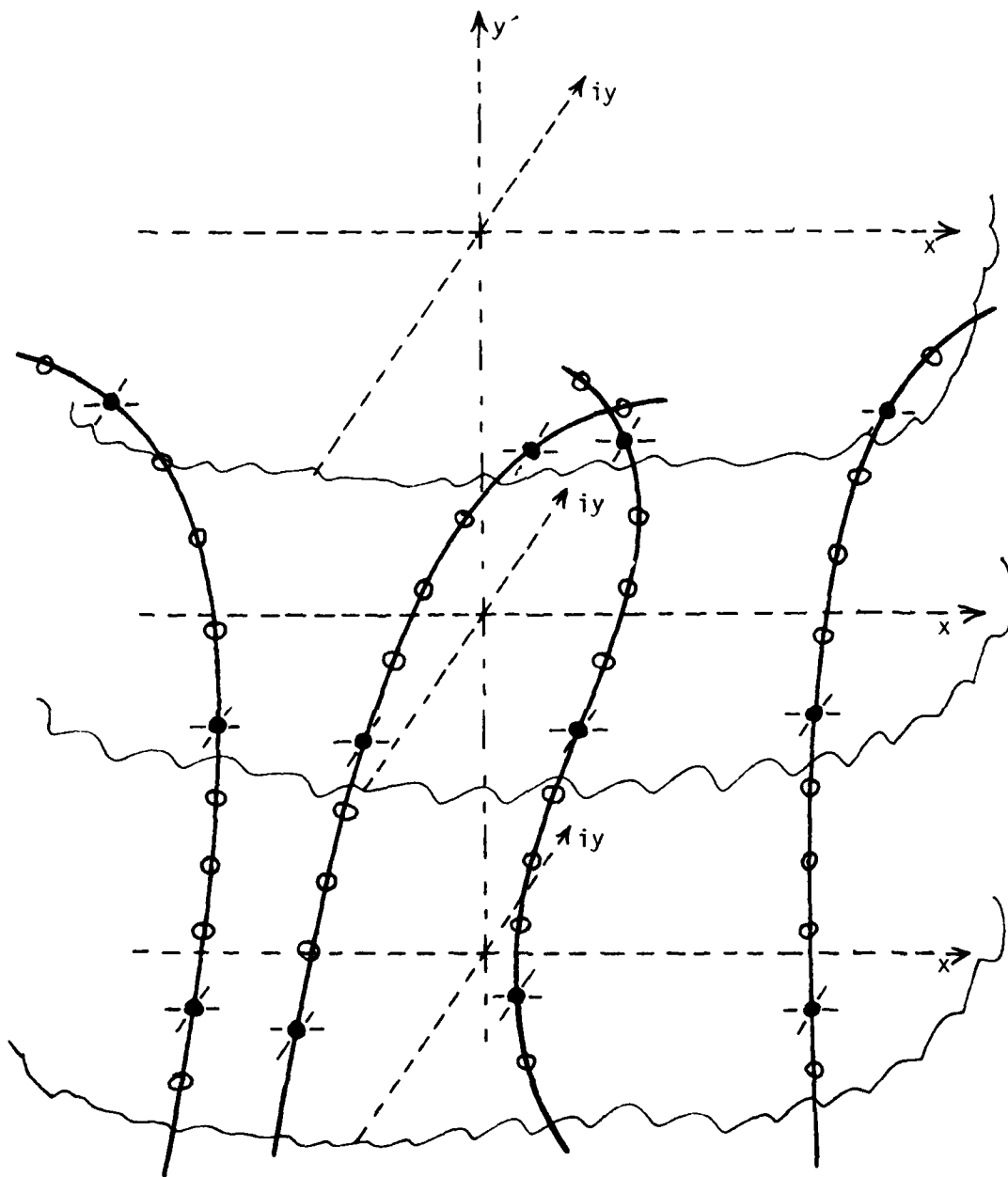


Fig. 9. Zeros of $A(z, y')$

$h(x,y) = h(x)$. Even if the Fourier transform of $A(z=x,y)$ leads to an unsatisfactory $p(u,v)$, it can be expected to provide a good starting $|p(u,v)|$ for the iterative phase construction algorithm discussed in section 4.1.4.

4.1.3 The Feasibility of Large-Scale Optimization

Given $h(x,y)$, is it possible to find a least square fit $h'(x,y)$ by optimizing parameters in the pupil? If $h(x,y)$ has very little detail, and may be represented by a few samples, $h(i,j)$, and $p(u,v)$ may also be adequately represented by a few samples $p(n,m)$. Optimization in ten variables can be done rather easily by computer, but the computation time for unstructured optimization increases as the square of the number of variables, and so the largest problems solvable with general purpose optimization routines like Fletcher-Powell on today's computers must have fewer than 200 variables.³¹ Unfortunately, optical processing has an advantage only when large amounts of data is to be processed, and therefore we are interested in $h(x,y)$ which must be represented by millions of variables! Thus we would need to solve an optimization problem that is one hundred million times larger than the largest problems feasible. It is clear that brute force optimization procedures are useful only on small test problems that might be of interest in benchmarking other approaches; however, selective use of optimization in conjunction with other techniques remains a strong option (Section 4.2.2).

4.1.4 Gerchberg-Saxon Iteration

Given $h(x,y)$ and a guess for $|p(u,v)|$, a technique originated by Gerchberg and Saxon²² is applicable. A reasonable choice is $|p(u,v)| = 1$ within the open aperture of the imaging lenses, and $|p(u,v)| = 0$ outside, because this choice corresponds to the most efficient possible pupil function. This, of course, is no guarantee that the iterative algorithm will converge to a solution, because the given $h(x,y)$ may be inconsistent with $|p(u,v)| = 1$.

The principle behind the Gerchberg-Saxon iteration is that the phase function over the pupil affects the output intensity distribution $h(x,y)$. The given $h(x,y)$ therefore contains implicit information about the phase $\phi(x,y)$ of $p(u,v)$. The problem is to combine this implicit phase information with $|p(u,v)|$. Gerchberg and Saxon proceed iteratively (Fig 10): Choose a random initial phase $\theta_1(u,v)$ for $p_1(u,v) = |p(u,v)| \exp(i\theta_1(x,y))$. Compute $A_1(x,y) = |A_1(x,y)| \exp(i\phi_1(x,y))$ from Eq. (8). The error in θ , causes an error in both $|A_1(x,y)|$ and $\phi_1(x,y)$. Correct $|A_1(x,y)|$ by replacing it with $\sqrt{h(x,y)}$. Compute a revised pupil phase $\theta_2(u,v)$ by Fourier transforming $\sqrt{h(x,y)} \exp(i\phi_1(x,y))$. This cycle from the pupil plane to the output plane and back has the effect of injecting into $\theta_2, \theta_3, \dots, \theta_j$, the phase information which is implicitly contained in $h(x,y)$. Although the iteration may not converge to a pupil function which accurately produces an output intensity of $h(x,y)$, it can be shown that the mean-squared error between the estimates $h_j(x,y)$ and $h(x,y)$ reduces (perhaps only infinitesimally) with each iteration. In the process, $\theta_j(u,v)$ and $\phi_j(x,y)$ also become more accurate. Fienup has devised an over-relaxation technique which speeds up convergence, and has achieved some impressive results on related problems.^{21,32}

4.1.5 Dallas' Algebraic Approach

An approach which directly combines the information provided by $h(x,y)$ with the information provided by $|p(u,v)|$ was developed by Dallas.³³ The procedure is algebraic, and works with samples of $h(x,y)$ and $|p(u,v)|$. A criterion related to that of Nyquist is used to determine the sampling interval. First, all of the information is gathered into the pupil domain by applying a DFT (Discrete Fourier Transform) to $h(i,j)$. In analogy to Eq. (5), one obtains the autocorrelation of $p(m,n)$:

$$H(\ell,k) = \sum_{m,n} p(m+\ell, n+k) p^*(m,n) \quad (15)$$

Together with the given values of $|p(m,n)|$, Eqs. (15) may be progressively solved for $p(m,n)$. At each step, choices are encountered which may lead to alternate consistent solutions for $p(m,n)$. We view this as a strong

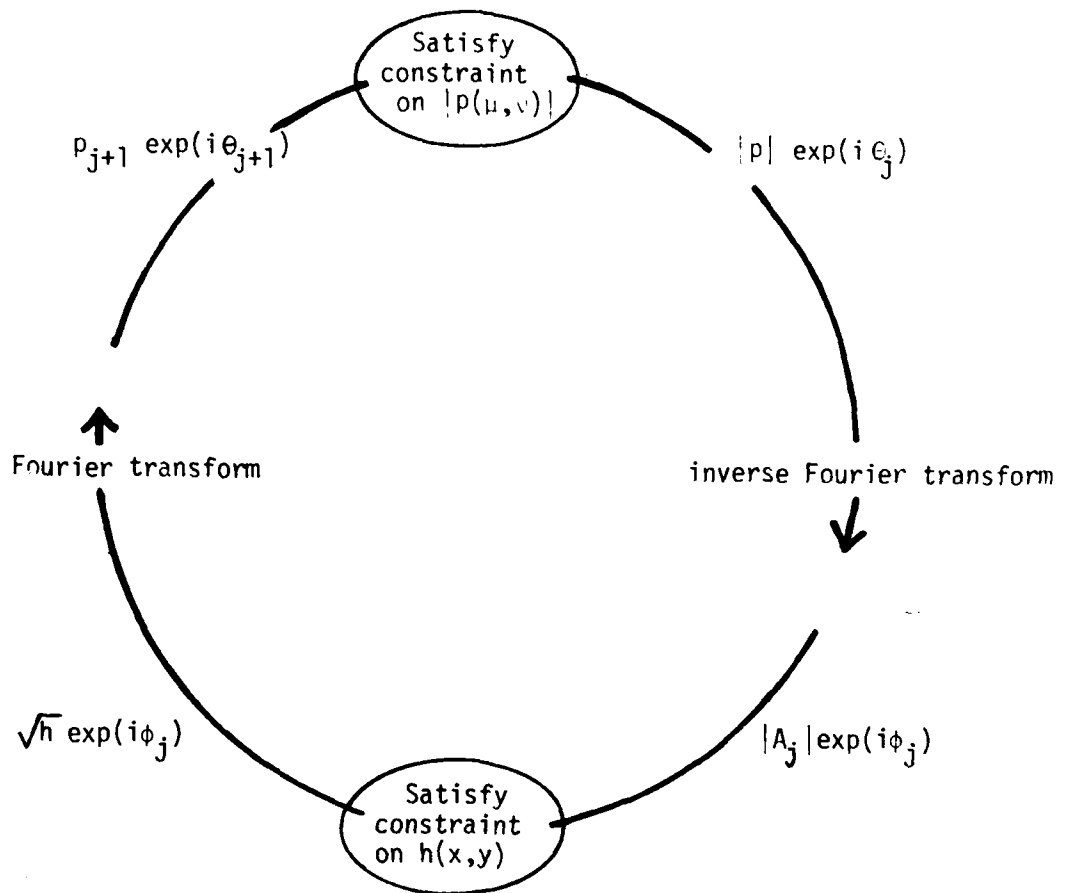


Fig. 10. Gerchberg-Saxon Iteration

point of the approach, because it leads to all possible solutions for the pupil function. The procedure has been carried out by hand on small 1-D test cases. However, we have found no reports of its successful application on large 2-D problems.

4.2.1 A Phase Determination Method from X-ray Crystallography

The probability of x-rays scattering in matter is proportional to the electron density localized around nuclei. The far field x-ray scattering amplitude is given by the Fourier transform of this atomic charge density; however, it is feasible only to record the magnitude squared of the Fourier transform. This loss of phase information precludes the straightforward calculation of atomic structure by inverse Fourier transformation of diffraction data. Crystallographers (Sayre,³⁴ Karle and Hauptman³⁵) dealt with this problem by developing approximate methods of phase determination. One of these methods is based upon the following facts: Electronic charge density is nonnegative and concentrated about nuclei. There is a negligible charge density in-between nuclei. In materials composed of the elements H, O, N and C, the x-ray scattering is due almost entirely to the O, N and C, which have larger atomic numbers than H. To a good approximation, the electronic charge density functions of O, N and C may be taken as identical, since they have adjacent atomic numbers. This "universal" electron charge density function $\rho(x,y,z)$ may be scaled so that it varies from 0 to a peak value of 1. Observe then that

$$\rho(x,y,z) \approx (\rho(x,y,z))^2. \quad (16)$$

The major effect of squaring is to narrow the distribution, without altering its peak value of 1 or its minimum value of 0. It can be shown that Eq. (16) leads to a tendency for the phase $\phi(x,y,z)$ of the x-ray scattering amplitude $F(x,y,z) = |F| \exp i\phi$ to obey the following relationship:

$$\phi(x+x', y+y', z+z') \approx \phi(x,y,z) + \phi(x',y',z') \quad (17)$$

This relationship is of considerable aid in determining crystal structure from x-ray diffraction patterns. One begins by choosing the phases of three x-ray diffraction pattern peaks arbitrarily. (This merely establishes a linear phase variation across the pattern, which one is free to choose at will.) Then the peaks of most of the other peaks are filled in using Eq. (17). This procedure generates a trial scattering amplitude which is inverse Fourier transformed to provide a crude indication of the electronic density function. In combination with a knowledge of chemical bond angles and lengths, this crude density function is often sufficient to completely determine the structure.

Our application of the phase relationship Eq. (17) is based upon the resemblance of $\rho(x,y,z)$ with the intensity representation of PN codes (Fig. 11). PN codes consist of a deterministic, yet seemingly random sequence of +1s and -1s. Since intensity is nonnegative, PN codes must be represented in noncoherent optical processors by the presence or absence of a light pulse. Long codes may be arranged in 2-D for such operations as correlation or spectral analysis by means of a raster (Spann,³⁶ Thomas³⁷). The discrete nature of such an array of pulses carries over into Fourier space; both $h(x,y)$ and $p(\mu,\nu)$ possess a discrete lumpy texture. Suppose that $p(\mu,\nu)$ is also restricted to be real and nonnegative; then the phase relationship of Eq. (17) should apply. Rather than assigning a fixed phase to the $A(x,y)$ representing a 2-D spread spectrum code array $h(x,y)$, the phase is allowed to vary from pulse to pulse, so as to minimize the amplitude in-between pulses. As in the analysis of x-ray diffraction patterns, the phases of three pulses are chosen at will, and the phases of the remaining pulses are assigned by means of Eq. (17). Because this choice of phase is consistent with a nonnegative $p(\mu,\nu)$, it corresponds to an $h(x)$ which has a bright central "dc" peak. This undesirable feature is eliminated by defining a phase only pupil $p'(\mu,\nu)$ which varies from a phase of π to a phase of 0 wherever $p(\mu,\nu)$ changes from 0 to 1.

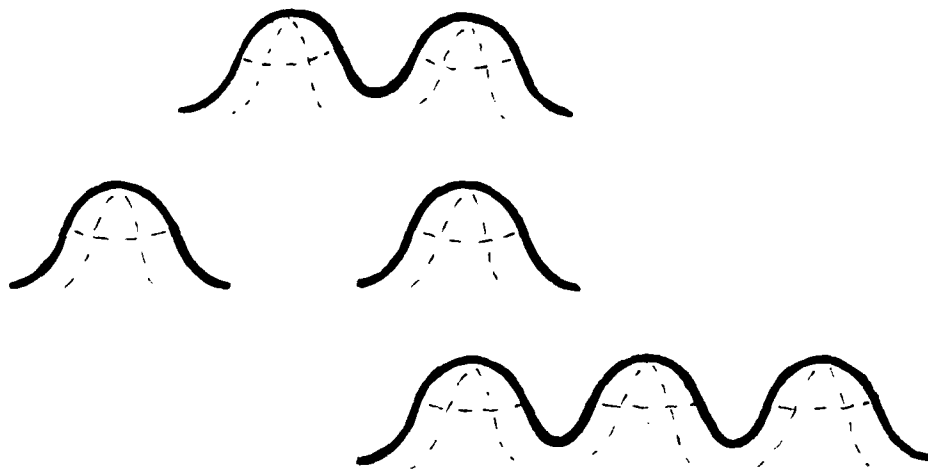


Fig. 11. Intensity representation of a PN code in a Two Dimensional Format.

4.2.2 Windowing in Conjunction with Small Scale Optimization

The initial goal of our work with noncoherent optical processing is to develop a technique for correlating the PN codes used in spread spectrum communication. Achievement of this goal would facilitate the acquisition and decoding of the long code sequences needed for low probability of intercept communications.³⁸ In such applications $h(x,y)$ will have the general form depicted in Fig. 11. This specific type of impulse response is naturally viewed as a superposition of elementary pulses. It is tempting to further imagine that the corresponding amplitude $A(x,y)$ is also composed of a superposition of pulses whose (universal) profile is tapered to zero a short distance away from the pulse center. We have examined this basic approach, and consider it a practical approach to the generation of pupil functions for PN code correlation. It is necessary, however, to refine the basic idea by choosing an optimal pulse shape (or equivalently choosing the optimal window function in the pupil), and by introducing a method of optimally choosing the phase of each elementary pulse, so that the overlapping tails of near-by pulses do not add up and produce an unwanted contribution to $h(x,y)$.

It is desirable to choose a pulse profile that is highly concentrated, and has negligible tails. However, the pulse must also be bandlimited, because it is created by a pupil of finite width. Due to the uncertainty principle it is not possible to have an arbitrarily narrow main lobe, or arbitrarily low sidelobes. A trade-off must be made between these desirable properties. We list a few of the possible window choices and their special features below. One of the most interesting choices is the prolate spheroidal window, because its maximal energy concentration property is an attractive feature for the pulses making up $h(x,y)$.

4.2.2.1 Prolate Spheroids

A prolate spheroidal window over the pupil aperture provides the greatest concentration of energy possible within a given interval in the output plane.³⁹ A problem with prolates is that there can be many ripples in the output plane interval where the energy is maximally concentrated.

4.2.2.2 Taylor Approximation to Dolph-Chebyshev Windows

This class of windows provides a narrow main lobe, but does not dissipate most of the energy into the sidelobes as ordinary Dolph-Chebyshev windows do.⁴⁰ The m sidelobes are of equal amplitude; after these they fall off as $1/x$.

The parameter m can be adjusted to control the fraction of total energy going into the main lobe, and also to control the width of the main lobe for a given maximum sidelobe level.

4.2.2.3 Raised Cosine + Pedestal Windows

This class of windows are reasonable good and also simple to compute. For example, a cosine raised to the second power + a pedestal is only 20% worse than the optimal Dolph-Chebyshev window as measured by the criteria of minimum main lobe width for a specified peak sidelobe level.⁴⁰

The sidelobes can be made to drop off arbitrarily fast by increasing the power to which the cosine is raised; for cosines raised to the $n-1$ power, the sidelobes fall off as $1/x^n$.

4.2.2.4 Optimizing Pulse Phase

It is easy to argue that the phases of each superimposed amplitude pulse should be carefully chosen, in order to make the most use out of the amplitude interferences which contribute to $h(x,y)$. Consider first the case of two adjacent pulses. If they have the same phase, they will reinforce along their border, and produce an undesirable overshoot in $h(x,y)$. If they have a phase difference of π , an unshoot occurs. But if they have a phase difference of $\pi/2$, they do not interfere at all. Consider the case of superimposed amplitudes A and $i\epsilon$. They combine to produce an intensity $(A+i\epsilon)(A-i\epsilon) = A^2 + \epsilon^2$, which is exactly the same value as the sum of their individual contributions A^2 and ϵ^2 . In other situations it may be desirable for pulses to have phases that reinforce, or phases that cancel. If the choice of a particular pulse phase had a global effect, A large scale optimization problem would need to be solved, and we have seen that (Section 4.1.3) this is not feasible. Fortunately, by choosing

a pupil window function which causes the pulse tails to rapidly taper to zero, we restrict the region affected to the immediate neighborhood of the pulse. One possible approach is to pick one corner of $h(x,y)$, and use an optimization routine to jointly optimize the phases of, say, 16 pulses. These phases are then fixed, and used as a boundary condition for the optimization of an adjacent set of 16 pulses, and so forth, until all of the phases are optimized locally. While not yielding the absolute best approximation to a given $h(x,y)$ this procedure promises to come very close, because it takes the most significant phasing effects into account.

4.3 Computer Generated Holograms for Pupil Masks

The feasibility of using the AFGL CRT plotter (a Calcomp 1675) to make Computer Generated Holograms (CGH) was investigated. The limiting resolution observed on 35 mm film was roughly 1,700 line pairs both vertically and horizontally. This is more than enough resolution for making ROACHs (Section 4.1).

The spatial distortion of the CRT was analyzed using a moire technique. The CRT was used to plot horizontal and vertical gratings. The 35 mm recordings of these gratings were then tested against a master Ronchi possessed by SAI. A small amount of barrel distortion was measured. If this distortion is a permanent feature, it can be easily bucked-out by pre-distorting the command coordinates supplied to the CRT. If we choose a scale (Fig. 5) such that the CRT display goes from -1 to +1 in both the x (across the film length) and y (along the film length) directions, then the barrel distortion will be greatly reduced by replacing x by:

$$x - (.0051)xy^2 - (.0136)x^3$$

and replacing y by:

$$y - (.0039)yx^2 - (.0149)y^3.$$

5. Image Pickup Devices

Noncoherent optical processing imposes a different set of requirements on detectors than does coherent optical processing. A linear response with intensity (i.e. $\gamma = 1$) is needed, rather than the sublinear ($\gamma = .5$) response ideal in most coherent processing applications. This difference arises because signals are represented by intensity in noncoherent optics, while they are represented by amplitude in coherent optics.⁴¹ Generally, a greater emphasis must be placed on sensitivity in noncoherent optics, because many noncoherent light sources (e.g. low pressure mercury arc lamps, or rare-earth phosphor cathode ray tubes) do not have the intensity of lasers. Since it is also likely that a mercury arc lamp will be used in some tests of the processor, it is important that the spectral response of the detector be high at the green mercury line ($\lambda = .546$ micron), as well as at the wavelength of a HeNe laser ($\lambda = .633$ micron). Finally, higher spatial resolution is needed in noncoherent optical processing, because spatial carriers may be used to the encode phase information utilized in post-detection electronic processing.⁴²

The ideal image pickup device would have no spatial distortion. Detector array devices such as CCD or CID cameras offer this desirable feature. However, at present these cameras do not provide the resolution available from vidicons. For this reason, we surveyed the available types of vidicons to assess their relative merits. The data collected and computed from manufacturers specifications is tabulated in Table 2. The quantum efficiency ratings proved to be most elusive. Manufacturers⁴³ do not provide quantum efficiency data, but it is (painstakingly!) possible to compute quantum efficiencies from the data usually furnished on specification sheets. It is standard to find (1) the relative spectral response of the vidicon target, and (2) the absolute sensitivity in mA/watt for specific broadband illumination -- usually expressed in lumens/square foot from a tungsten lamp at 2856⁰K. The lumen is a psychophysical unit, (which makes sense in most applications of vidicons) and it is necessary to convert over to

Table 2

Comparison of Vidicon Target Materials

<u>Target Material</u>	<u>Quantum Efficiency at .546 micron*</u>	<u>Y</u>	<u>Dark Current (half inch vidicon)</u>
SbS ₃ (RCA)	12%	.65	5-20 nanoamps
Se-Te-As (Saticon)	28%	1.0	.3 - .5 nonoamp
CdSe ? (Chalnicon)	95%	.95	1 nanoamp
PbO (Amperex)	57%	.95	1.5 - 3 nanoamps
Si (RCA)	83%	1.0	8.5 nanoamp

* For some undetermined reason, these values are all unrealistically high. They should still be useful for comparisons.

physical units using the spectral response of the photopic eye, the spectral characteristics of the tungsten lamp. The tungsten lamp spectrum is computed from the Stefan-Boltzmann law and the emissivity of tungsten. By integrating the lamp spectrum as weighted by the spectral response curve provided by the manufacturer, this response curve may be calibrated in terms of its quantum efficiency -- electrons out/photons in. One of the reasons that manufacturers do not specify quantum efficiency is that many vidicon target materials have a nonlinear response versus intensity ($\gamma \neq 1$). In such cases, we computed an effective quantum efficiency about the illumination level used by the manufacturer to specify the absolute sensitivity of the target.

From the data in Table 2, it is clear that the best vidicon target materials for noncoherent optical processing are CdSe or Si. Both materials offer high quantum efficiency at .546 micron, and both have nearly linear response with intensity ($\gamma = 1$). The CdSe target comes out ahead of the Si target because it also offers a higher resolution and a slightly lower dark current. As this comparison covers only three of a multitude of other potentially important criteria, other types of vidicons may be better suited in specific noncoherent processing applications. For example, the Saticon target absorbs light strongly, and this reduces the problem of spurious imagery caused by light which first reflects off of the vidicon and then rebounds from another surface.⁴⁴

6. System Integration

In the applications of most interest, the optical processor must have an adaptive capability to respond to changes in signal or background character. This feature may be incorporated by adding a digital processor to oversee the optics. For example, in spread spectrum code acquisition and decoding, this digital processor might be a clock and a code box which alters the optical processing function in accord with scheduled shifts in the transmitted code pattern. Alternatively, the digital processor might be truly adaptive, and derive its cues from the signal level or character at the output of the optical processor (Fig. 12).

The optical processor subsystems (input device, pupil mask, output device) must also be linked together by a "housekeeping" system in order that component drift (with age or temperature) does not go unchecked, and introduce saturating signal levels, or spatial distortion in the input or output devices. Although these housekeeping tasks may be done digitally, they basically require simple analog electronic feedback or phase-locked loop circuitry. Since this topic is covered at length in one of the publications prepared under the contract, it is not necessary to go over the same ground here.⁴²

Alterations in the processor function may be achieved by changing the input scale or format, by changing the pupil mask or illumination wavelength, or by changing the post processing electronics. Consider, for example, the search for a known waveform (with known Doppler) which is buried in noise. The Doppler may be accommodated by adjusting the scan rate of the input device, because Doppler simply re-scales the waveform. Alternatively, the input scan rate may be held fixed, and the illumination wavelength may be varied, because the optical impulse response $h(x,y)$ and the optical filter function $H(f_x, f_y)$ scale with λ (Eg. 3, 4 and 5).⁴² These tricks provide considerable processing flexibility without actually switching the pupil mask itself. Applications like spread spectrum code acquisition and

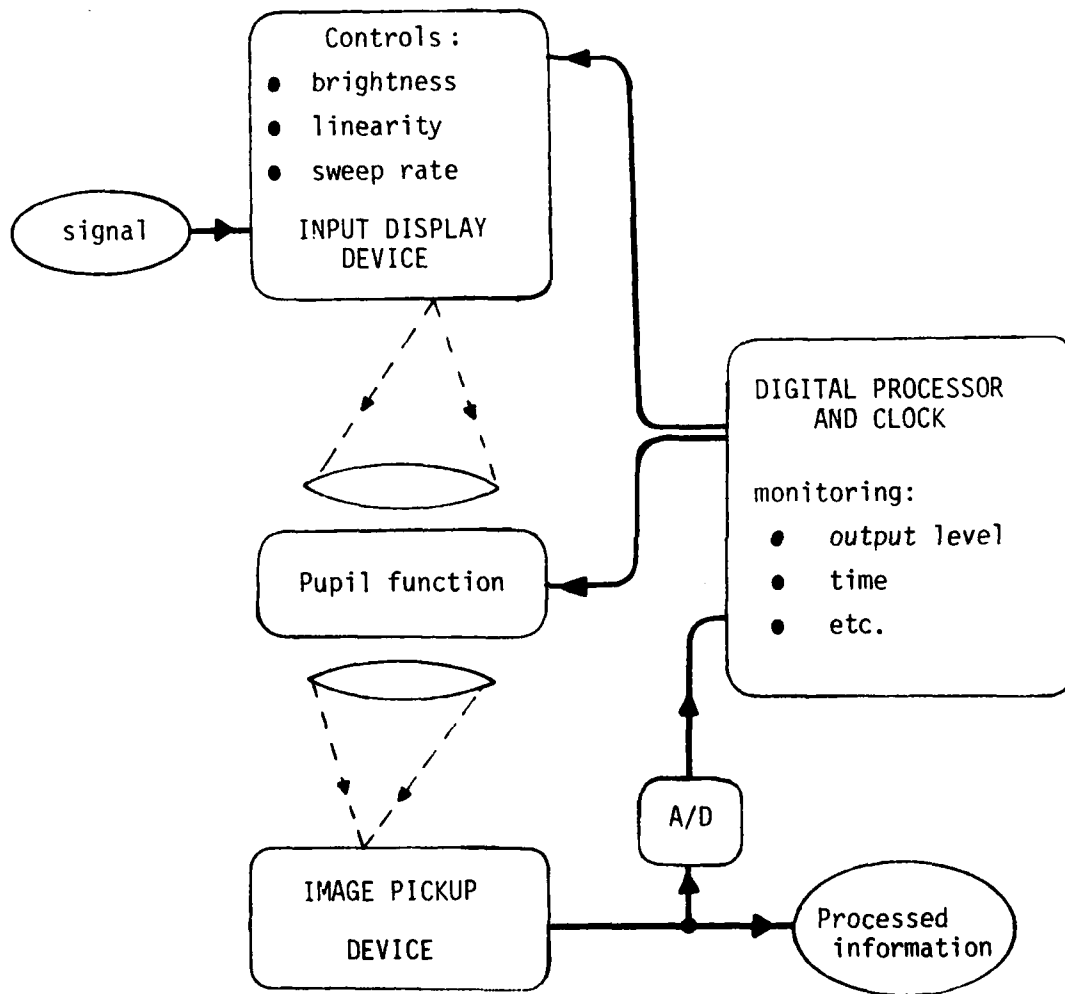


Fig. 12. Architecture for Adaptive Processing.

decoding, however, require the capability of switching from one pupil mask to another, and because codes change rapidly, it is not acceptable to represent them all in frozen form on a fixed pupil mask. Rather, it will be necessary to store or generate the appropriate pupil functions electronically, and to form pupil masks in real-time by means of a programmable light valve located in the pupil plane.

It is also possible to electronically switch between two processing functions without using a programmable light valve. This capability might have application in a binary code-switching communication system. The possibility comes about because a given filter function $H(f_x, f_y)$ has distinct even and odd components,

$$H_e(f_x, f_y) = \frac{1}{2} (H(f_x, f_y) + H(-f_x, -f_y))$$

Eq (18)

$$H_o(f_x, f_y) = \frac{1}{2} (H(f_x, f_y) - H(-f_x, -f_y)).$$

H_e controls the cosine components of the output image, while H_o controls the sine components. During the post-detection operation of coherent demodulation, these two image components are isolated, making it feasible to electronically select either the filter function H_e or H_o .

Another technique which permits the processing function to be switched electronically is to partition each separate function in non-overlapping bands of spatial frequency. That is, the filter function of the processor, $H(f_x, f_y)$, is chosen to contain an array of M sub-filters each with its own frequency cell and center frequency, (f_{xi}, f_{yi}) , $i = 1$ to M . A given one of the M sub-filters is selected by heterodyning the input signal in spatial frequency by (f_{xi}, f_{yi}) , so that it is centered in the frequency domain about the i th sub-filter. On post-detection electronic processing, the filtered signal is "re-centered" in frequency space by heterodyning with $(-f_{xi}, -f_{yi})$, and then bandpass filtered to eliminate the effects of the other $M-1$ subfilters. This approach is acceptable only if the spatial frequency bandwidth of the processor optics is adequate to represent all of the M processing functions. The reader may be puzzled by the meaning of a frequency shift

(f_{x_i}, f_{y_i}). If an image is raster scanned with the fine scan axis oriented along the x direction, heterodyning by $\exp(-2\pi x f_{x_i})$ will shift the spatial frequency of the raster signal to (0, f_{y_i}). Successive scan lines, $n = 1, 2, 3, \dots$, are then shifted to (0,0) by multiplying by the phase factor $\exp(-2\pi n \delta f_{y_i})$ where δ is the distance along the y direction separating adjacent scan lines. This combined operation may be implemented electronically by means of a raster line counter and digital phase-locked loops.

7. Contributors

- (1) William Stoner, principal investigator
- (2) Edward Garber, pupil mask design
- (3) Frank Horrigan, signal processing
- (4) Glenn Collins, optical design
- (5) John Phelps, programming

8. List of Publications, Presentations
and Related Contracts

8.1 Publications supported in part or in whole by this contract

- 1) "Optical Processing with the OTF," published in the International Optical Computing Conference Digest of papers, (Institute of Electrical Engineers, Inc., 1978), pp 172-175, 5 Sept. 1978.
- 2) "Incoherent Optical Processing via Spatially Offset Pupil Masks," Applied Optics, 17, 15, pp 2454-2467, 1 Aug. 1978.
- 3) "System Roles for Noncoherent Optical Processing," to be published in SPIE Vol. 209, Optical Signal Processing for Command, Control, Communications and Intelligence.

8.2 Presentations supported in part or in whole by this contract

- 1) "Optical Analog to Digital Conversion," Gordon Conference on Coherent Optics and Holography, 21 June 1978.
- 2) "Optical Processing with the OTF," International Optical Computing Conference, City University, London England, 5 Sept. 1978.
- 3) "Spread Spectrum," Seminar on Optical Signal Processing and C³ Applications, Hanscom Air Force Base, Bedford, MA, 13 July 1978.
- 4) "Noncoherent Optical Processing," Invited presentation and panel discussion on optical signal processing, 1978 Optical Society of America meeting, San Francisco, CA, 30 Oct. 1978.
- 5) "System Roles for Noncoherent Optical Processing," presentation scheduled for 30 Oct. 1979 before the Rome Air Development Center sponsored conference on Optical Signal Processing for C³I, Newton, MA.

8.3 Related and Previous Contracts

- 1) F19628-77-C-0110 previous contract with RADC/ET
- 2) DASG60-78-C-0136 related contract with the Ballistic Missile Defense Advanced Technology Center (Sept 1978 to June 1979).

9. References

1. A. W. Lohmann, *Applied Optics*, 16, p. 261 (1977).
2. W. T. Rhodes, *Applied Optics*, 16, p. 265 (1977).
3. W. Stoner, *Applied Optics*, 16, p. 1451 (1977).
4. M. A. Monahan, K. Bromley, and R. P. Bocker, *Proc. IEEE*, 65, p. 121 (1977).
5. Personal communication, Dr. Freeman Shepherd RADC/ET, Hanscom AFB.
6. G. Pietri, *IEEE TRans. NS-24*, 1, p. 228 (Feb. 1977).
7. E. A. Trabka and P. G. Roetling, *Journal of the Optical Soc. Am.*, 54, 10, p. 1242, (Oct. 1964).
8. Joint Electron Device Engineering Council, Optical Characteristics of Cathode Ray Tube Screens, Electronic Industries Association, 2001 Eye St. N.W., Washington, D.C. 20006, Nov. 1975, p. 82.
9. Reference 8, p. 16.
10. P. M. Heyman, I. Gorog, and B. Faughnan, *IEEE Trans. ED-18*, 9, (Sept. 1971), pp. 685-691.
11. I. F. Chang and A. Onton, *Journal of Electronic Materials*, 2, 1, 1973, pp. 17-46.
12. P. Chavel, Traitement optique en éclairage incohérent théoriques et limitations expérimentales, thesis, Université de Paris-sud, (1978).
13. J. R. Packard, J. M. Magnusson, H. V. Brueckner, and W. H. Strodon, *Optical Engineering*, 14, 3, (May-June 1975) pp. 248-250.
14. P. J. Brosens, *Applied Optics*, 11, p. 2987, (Dec. 1972).
15. A. V. Oppenheim and R. W. Schaffer, Digital Signal Processing, (Prentice-Hall, Inc., Englewood Cliffs, N.J., 1975).
16. R. H. Tancrell, *IEEE Trans. SU-21*, 1, p. 12, (Jan. 1974).
17. E. L. O'Neill, Introduction to Statistical Optics, (Addison-Wesley, 1963).
18. E. L. O'Neill and A. Walther, *Optica Acta*, 10, p. 33 (1962).

19. J. Tsujiuchi, "Correction of Optical Images by Compensation of Aberrations and by Spatial Filtering," Vol II, Progress in Optics (North Holland, 1963). pp. 131-180.
20. D. C. Chu, J. R. Fienup, and J. W. Goodman, Applied Optics, 12, p. 1386 (1973).
21. J. R. Fienup "Improved Synthesis and Computational Methods for Computer Generated Holograms," Thesis, Stanford Univ. 1975, (Xerox University Microfilms, Ann Arbor, MI).
22. R. W. Gerchberg and W. O. Saxon, Optik 35, p. 237 (1972).
23. W. Stoner, Applied Optics, 17, p. 2454 (1978).
24. E. L. O'Neill and A. Walther, Optica Acta, 10, p. 33 (1962).
25. A. Walther, Optica Acta, 10, p. 41 (1962).
26. E. M. Hofstetter, IEEE Trans. IT-9, p. 119 (1963).
27. M. Goldberger, H. Lewis, and K. Watson, Phys. Rev., 132, p. 2764 (1963).
28. C. P. Slichter, Principles of Magnetic Resonance, (Harper and Row, New York, N.Y., 1963) p. 38.
29. H. W. Bode, Network Analysis and Feedback Amplifier Design, Chapter XIV, "Relations Between Real and Imaginary Components of Network Functions," pp. 303-336, (Fourteenth Printing, Robert E. Krieger Publishing Co., Inc., Huntington, N.Y., 1975).
30. Reference 15, pp. 346-353.
31. D. G. Luenberger, Introduction to Linear and Nonlinear Programming, (Addison Wesley, 1965).
32. J. R. Fienup, Optics Letters, 3, 1, p. 27, (July 1978).
33. W. J. Dallas, Optik, 44, 1, p. 45 (1975).
34. D. Sayre, Acta Cryst. 5, p. 60 (1952).
35. J. Karle and H. Hauptman, Acta Cryst. 3, p. 181 (1950).
36. R. Spann, Proc. IEEE, 53, p. 2137 (1963).
37. C. E. Thomas, Applied Optics, 5, p. 1782 (1966).
38. R. C. Dixon, Spread Spectrum Systems, p. 6 (John Wiley, 1976).
39. B. R. Friedan, "Evaluation, Design and Extrapolation Methods for Optical Signals Based on Use of the Prolate Functions," Vol. IX, Progress in Optics (North Holland, 1971).

40. E. C. Farnett, T. B. Howard, and G. H. Stevens, "Pulse-compression Radar," chapter 20, pp. 20-26 to 20-34, Radar Handbook, I. I. Skolnik, Editor (McGraw-Hill, 1970).
41. Pointed out by Prof. J. W. Goodman of Stanford Univ. during panel discussion on optical processing at the 1978 Optical Society Meeting in San Francisco, CA.
42. W. Stoner, "Optical Processing with the OTF," International Optical Computing Conference, Digest of Papers.
43. Those manufacturers whose vidicons were studied include RCA, AmpereX, Toshiba and Matsushiba.
44. R. G. Neuhauser, Journal Soc. Motion Pict. and Tele. Eng. 87, 3 (March 1978).

MISSION
of
Rome Air Development Center

RADC plans and executes research, development, test and selected acquisition programs in support of Command, Control Communications and Intelligence (C³I) activities. Technical and engineering support within areas of technical competence is provided to ESD Program Offices (POs) and other ESD elements. The principal technical mission areas are communications, electromagnetic guidance and control, surveillance of ground and aerospace objects, intelligence data collection and handling, information system technology, ionospheric propagation, solid state sciences, microwave physics and electronic reliability, maintainability and compatibility.

ATE
LMED
-8